表 2 HIV 感染症患者に見られる悪性腫瘍

AIDS 指標悪性腫瘍（AIDS-Defining Malignancies ; ADM または AIDS-Difinining Cancers ; ADC）
・カポジ肉腫
・非ホジキンリンパ腫（中枢神経系，全身性）
・浸潤性子宮頸癌

非 AIDS 指標悪性腫瘍（Non-ADM, NADM または NADC）
・肛門癌
（HPV 関連悪性腫瘍）
・ホジキンリンパ腫
・原発性肺癌
・肝細胞癌
・精巣腫瘍（セミノーマ）
・頭頸部癌
・多発性骨髄腫，白血病
・皮膚癌（基底細胞癌，有棘細胞癌，メラノーマ）
・口腔癌，結膜癌など

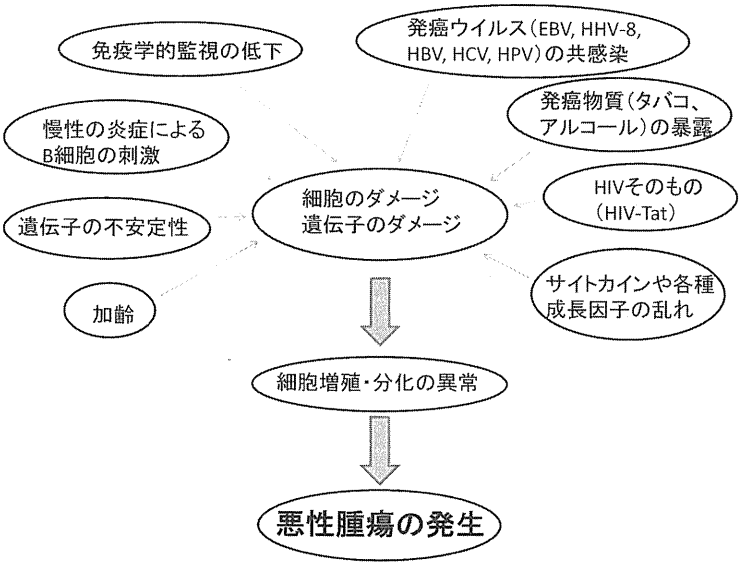

図 4 HIV 感染症患者における悪性腫瘍のリスク因子

またNADM患者の背景因子を解析してみると，AIDS発症群，CD4陽性リンパ球数の最低値が200未満，ART施行群，HIVと診断されて5年以上の群でHazard Ratioが高いことが報告されている[3]。さらにHIV感染症患者の死因として悪性腫瘍が増加していることも報告されている。以上のようにHIV感染症患者におけるNADMの問題はいわば不可避の状況になっている。

3. NADM発症にかかわる因子・原因

HIV感染症患者に悪性腫瘍が発生する原因は単一ではなく，さまざまな因子が複雑に関係している（図4）[4]。

HIV感染症患者では腫瘍免疫の低下，各種発癌ウイルス（EBV, HHV-8, HBV, HCV, HPV）の共感染，さらにHIVそのものの関与[5]や，HIV感染症患者での遺伝子の不安定性の頻度が高いこと[6]も指摘されている。他に環境的な要因として，タバコやアルコール，日光の暴露が挙げられる。特にタバコに関しては各種悪性腫瘍のリスク因子であるだけでなく，HIV感染症患者では非HIV感染症患者に比して喫煙率が高いことも悪性腫瘍の発症頻度の高さに寄与し

ているものと思われる。このようにさまざまなファクターが関わっており，多方面からの介入が重要である。

4. NADMの臨床的特徴と治療時（主に化学療法時）の注意点

NADMを併発したHIV感染症患者の臨床的な特徴，また実際に診療に関わる際の注意点として，非HIV患者に比して①より若年で発症，②高悪性度の腫瘍の頻度が高い，③進行期（遠隔転移を伴う）が多い，④治療に抵抗性で予後不良，が挙げられる。従って特に進行期の悪性腫瘍の場合は治療のメリット・デメリットを熟考し，治療方針を決定すべきである。

また実際の治療の際の問題点として，a）HIV感染症や合併症によるPSの低下があること，b）手術合併症の頻度増加のリスク（特にCD4陽性リンパ球低値患者），c）抗腫瘍化学療法による副作用（特に骨髄抑制）の頻度が高いこと，d）抗HIV薬と抗腫瘍薬の薬物相互作用があること，が挙げられる。抗腫瘍化学療法を行う際にはHIV感染症の治療も同時に行うことが重要である。またもともと免疫不全がある患者に抗腫瘍化学療法を行うことでさらなる免疫の低下が起こることから，抗腫瘍化学療法の際の感染症発症の頻度も高く，積極的な日和見感染症の予防や感染症発生時の迅速な対応が求められる。

抗腫瘍薬と抗HIV薬との薬物相互作用の詳細は割愛するが（文献[7]を参照），一般にプロテアーゼ阻害薬特にRTVは一部の抗腫瘍薬の代謝に関わるCytochrome P450 3A4（CYP3A4）の阻害作用を有しているため，併用することによってこの酵素で代謝される一部の抗腫瘍薬の血中濃度が上昇して重篤な副作用が生じる可能性がある。一方，非核酸系逆転写酵素阻害剤はCYP3A4を誘導し，併用する抗腫瘍薬の代謝を亢進させて血中濃度を低下させる可能性があることと，内服困難になった場合の耐性ウイルスの誘導が容易であること，服薬早期の副作用として発熱が出現することがある，などの点から，使用しにくいことが考えられる。

最近になって使用されるようになったインテグラーゼ阻害剤であるraltegravir（RAL）は相互作用も少なく，また服用に際し食事の影響を受けないことから抗腫瘍化学療法中に使用する抗HIV薬としては望ましいプロファイルを有していると言える。同様にCCR5受容体拮抗薬であるmaraviroc（MVC）も若干の相互作用の問題はあるものの有用であろう。いわゆるキードラッグとしてはこれらの薬剤が実際的と思われる。

HIV感染症患者に発症した悪性腫瘍の治療の際はHIV感染症だけでなく腫瘍学にも通じた専門家のもとで行うべきであるといえる。

5. おわりに

HIV感染症に伴うNADMについて概説した。この問題は患者の高齢化などに伴いますますその重要度が増加していくことが想定される。NADMは非HIV感染症患者と同様に予防と早期発見が肝要であるが，確立されたスクリーニングプログラムはなく，いわゆる職場や自治体の健康診断や人間ドックに頼らざるを得ない。さらに，一般的なことであるが禁煙の指導や，定期的な健康チェックの推奨などが必要であろう。HIV診療に関わる者は，日和見疾患や生活習慣病にとどまらず悪性腫瘍の問題もありうることを認識すべきと思われる。また今後は悪性腫瘍発症にHIVそのものの関与もあることから，HIV感染症患者へのより早期からの抗HIV療法が求められるようなことも示唆される。

参考文献

1）The Antiretroviral Therapy Cohort Collaboration : Life expectancy of individuals on combination antiretroviral therapy in high-income countries : a collaborative analysis of 14 cohort studies. Lancet 372 : 293-299, 2008.

2）International Collaboration on HIV and Cancer : Highly active antiretroviral therapy and incidence of cancer in human immunodeficiency virus-infected adults. J Natl Cancer Inst 92 : 1823-1830, 2000.

3）Powles T, Robinson D, Stebbing J, et al : Highly active antiretroviral therapy and the incidence of non-AIDS-defining cancers in people with HIV infection. JCO 27 (6) : 884-890, 2009.

4）Barbaro G, Barbarini G : HIV infection and cancer in the era of highly active antiretroviral therapy (Review). Oncol Rep 17 (5) : 1121-1126, 2007.

5）Corallini A, Sampaolesi R, Possati L, et al : Inhibition of HIV-1 Tat activity correlates with down-regulation of bcl-2 and results in reduction of angiogenesis and oncogenicity. Virology 299 (1) : 1-7, 2002.

6）Wistuba II, Behrens C, Gazdar AF : Pathogenesis of non-AIDS-defining cancers : a review. AIDS Patient Care STDS 13 (7) : 415-426, 1999.

7）Spano JP, Costagliola D, Katlama C, et al : AIDS-related malignancies : state of the art and therapeutic challenges. J Clin Oncol 26 (29) : 4834-4842, 2008.

当センターにおける近年の肛門疾患手術症例の HIV 陽性例の変遷
—特に肛門管尖形コンジロームの検討—

佐原力三郎（社会保険中央総合病院　大腸肛門病センター）

A review of transition of the ratio of HIV positive patients who have been performed operation in our hospital in recent years
—Especially studied about patient with condyloma acuminatum of anal canal—

Rikisaburo SAHARA

1.　はじめに

当院・当センターでは年間 2000 例以上の肛門疾患手術を施行している。主な疾患内容は痔核，痔瘻，裂肛であり，その頻度は以前から大きな変化はないが，近年それらの症例において HIV 陽性患者が急増しており，中でも肛門管尖圭コンジローム症例において顕著となっている。

近年 9 年間を前半期（2001 年～2005 年）と後半期（2006 年～2009 年）に分けて検討を加えた。

2.　当院・当センターの特徴

中規模総合病院（病床数 418）の中に大腸肛門疾患を専門に診療する科として当センターが設立され 51 年が過ぎた。肛門疾患をはじめ大腸癌，炎症性腸疾患，大腸肛門機能性疾患などの，大腸肛門にかかわる疾患の外科的診療を専門的に行ってきている。総合病院の一角であるがゆえにいろいろな合併症を有する症例に対しても安全かつ積極的に治療を進めてきた。肛門疾患は良性疾患であるがゆえに合併症の重篤な症例に対し，他施設では手術療法は遠慮されがちであるが，適応を広げて診療してきている。HIV 陽性患者に対する肛門部観血的治療も扱う施設は限られるため，エイズ拠点病院（1997 年認可）である当院・当センターへの紹介例は少なくない。

3.　HIV 陽性手術症例数の年次推移（図 5）

前半期では 10877 症例の肛門疾患手術を施行し，男性 7061 例，女性 3816 例（男女比 1.9：1）であった。そのうち HIV 陽性例は 37 例で全員男性であった。男性症例の 0.52％にあたり 200 例に 1 人の割合であった。さらにこの期間の尖圭コンジローム手術症例数は 98 例であり，うち 17 例が HIV 陽性症例であった。約 6 例に 1 例の割合であった。

後半期になると，7758 症例の手術例のうち男性 6747 例，女性 3251 例（男女比 2.1：1）であり，HIV 陽性例は 121 例に増加し，この中に 1 例のみではあったが女性の痔瘻症例が認められた。HIV 陽性症例は全体では 1.6％で前半期との比較では 4.6 倍，男性の中では 1.8％となり前半期との比較では 3.4 倍，50 例中 1 例の割合に増加した。さらに尖圭コンジローム症例は 175 症例経験し，HIV 陽性例は 79 例（45％）であり前半期との比較では 3.4 倍と急増していた。175 例全て男性であり性行為感染症としての尖圭コンジロームであった。実に 2.2 例に 1 例の割合と著明であった。

4.　受診時の背景

後半期 HIV 陽性尖形コンジローム 79 例の当センター受診形態をみると，59 例（74.7％）が紹介であり，受診時すで

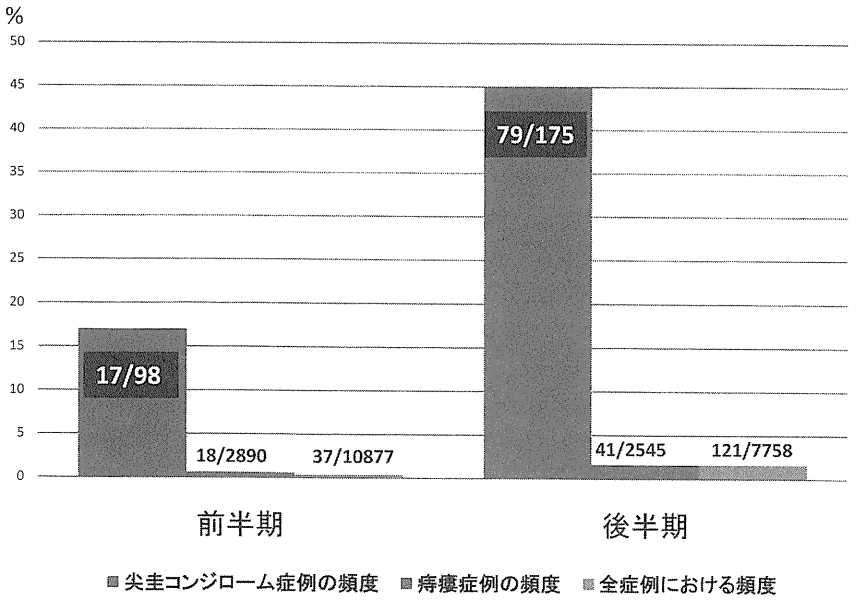

図 5　肛門疾患別 HIV 陽性頻度の比較

に患者本人がHIV陽性を知っていた症例は60例（75.9%）であった。逆に紹介元も知らず患者本人も知らない例，つまり新規届け出を要する例は19例（24.1%）であった。

5. 複数感染

後半期HIV陽性尖形コンジローム79例における他の感染症の状況を検討すると，TP（梅毒）陽性例27例（34.2%），HBV（B型肝炎）陽性例11例（13.9%），HCV（C型肝炎）陽性例1例（1.3%）であった。

6. まとめ

近年9年間の当センターで経験したHIV陽性肛門疾患症例について検討したところ，症例数は確実に急激に増加しており，特に肛門管尖形コンジローム症例に顕著であった。これらの症例は全てSTDとしてのHIV陽性例であり男性であった。またこのような症例では他のSTD感染特にTP，HBVの陽性率が高値であり，診療現場での注意喚起も必要かと思われた。

Virology xxx (2012) xxx–xxx

Contents lists available at SciVerse ScienceDirect

Virology

journal homepage: www.elsevier.com/locate/yviro

Novel monoclonal antibodies for identification of multicentric Castleman's disease; Kaposi's sarcoma-associated herpesvirus-encoded vMIP-I and vMIP-II

Kazushi Nakano [a,1], Harutaka Katano [c,1], Kenjiro Tadagaki [b], Yuko Sato [c], Eriko Ohsaki [a], Yasuko Mori [d,e], Koichi Yamanishi [e], Keiji Ueda [a,*]

[a] Division of Virology, Department of Microbiology and Immunology, Osaka University Graduate School of Medicine, 2-2 Yamada-oka, Suita, Osaka 565-0871, Japan
[b] Institut Cochin, Université Paris Descartes, CNRS (UMR 8104) Inserm U1016, Paris, France
[c] Department of Pathology, National Institute of Infectious Diseases, Tokyo, Japan
[d] Division of Clinical Virology, Kobe University Graduate School of Medicine, 7-5-1, Kusunoki-cho, Chuo-ku, Kobe, 650-0017, Japan
[e] Division of Biomedical Research, National Institute of Biomedical Innovation, Ibaraki, Osaka, Japan

ARTICLE INFO

Article history:
Received 29 August 2011
Returned to author for revision 2 October 2011
Accepted 11 January 2012
Available online xxxx

Keywords:
Kaposi's sarcoma-associated herpesvirus
Kaposi's sarcoma
Multicentric Castleman's disease
Viral macrophage inflammatory protein
vMIP-I
vMIP-II
Chemokine
KSHV
HHV-8

ABSTRACT

Recent studies have indicated that vMIP-I and vMIP-II play important roles in the pathogenesis of Kaposi's sarcoma-associated herpesvirus (KSHV)-related diseases due to the effects of these proteins on vascularization. We developed monoclonal antibodies against KSHV-encoded viral macrophage inflammatory protein-I (vMIP-I) and vMIP-II to study these expression profiles and reveal the pathogenesis of KSHV-related diseases. The MAbs against vMIP-I and vMIP-II reacted to KSHV-infected cell lines after lytic induction. Both vMIP-I and the vMIP-II gene products were detected 24 h post-induction with 12-*O*-tetradecanoylphorbol-13-acetate until 60 h in the cytoplasm of primary effusion lymphoma cell lines. In clinical specimens, both vMIP-I and vMIP-II gene products were detected in the tissues of patients with multicentric Castleman's disease. On the other hand, only vMIP-II was detected in a subset of Kaposi's sarcoma. We concluded that these antibodies might be powerful tools to elucidate the pathogenesis of KSHV-related diseases.

Introduction

Kaposi's sarcoma-associated herpesvirus (KSHV), also known as human herpesvirus 8 (HHV-8), is a gammaherpesvirus originally identified in HIV-positive Kaposi's sarcoma (KS) tissues (Chang et al., 1994). KSHV is responsible for AIDS associated cancers such as Kaposi's sarcoma (KS), primary effusion lymphoma (PEL), and multicentric Castleman's disease (MCD) (Cesarman et al., 1995; Schalling et al., 1995; Soulier et al., 1995). As is the case for all herpesviruses, KSHV has two life cycles, one latent and the other lytic. Lytic gene expression can be induced by the treatment of latently infected cells with chemical agents such as 12-*O*-tetradecanoylphorbol-13-acetate (TPA), sodium butyrate (Arvanitakis et al., 1996; Miller et al., 1997). It has been demonstrated that two KSHV-encoded chemokines, K6 (which encodes a vMIP-I) and K4 (which encodes a vMIP-II), are expressed in the course of lytic infection (Moore et al., 1996; Sun et al., 1999). Previous reports showed that both vMIP-I and vMIP-II induced Ca^{2+} signal transduction via certain chemokine receptors and the receptor-dependent migration of cells (Benelli et al., 2000; Chen et al., 1998; Endres et al., 1999; Kledal et al., 1997). In addition, in a chick chorioallantoic membrane assay, the both proteins showed strong angiogenic properties (Boshoff et al., 1997). However, little is known about the contribution of vMIPs to KSHV malignancy under physiologic conditions.

In this report, we generated new monoclonal antibodies against vMIP-I and vMIP-II, and confirmed the detection of both vMIP-I and vMIP-II in histological sections of tissues from MCD patients as well as in KSHV-infected PEL cell lines. In cases of KS, vMIP-II was detected, but not vMIP-I. These results suggest that the expression properties of vMIP-I and vMIP-II might be related to KSHV-associated diseases, and may even be involved in the generation of diseases. Thus, antiviral chemokine MAbs could potentially become useful tools for the diagnosis of KSHV-related diseases.

Materials and methods

Cells

Kaposi's sarcoma-associated herpesvirus-positive cell lines (BC-1, BC-3, BCBL-1 and TY-1 cells) and a negative cell line (BJAB cells) were

* Corresponding author. Tel.: +81 6 6879 3780; fax: +81 6 6879 3789.
E-mail address: kueda@virus.med.osaka-u.ac.jp (K. Ueda).
[1] Equal contribution by these authors.

0042-6822/$ – see front matter © 2012 Elsevier Inc. All rights reserved.
doi:10.1016/j.virol.2012.01.008

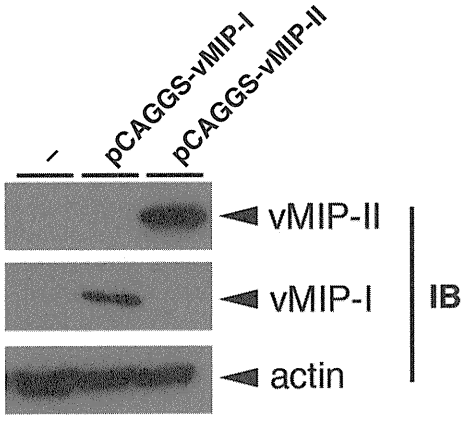

Fig. 1. Cross reactivity between anti-vMIP-I and anti-vMIP-II MAb. 293 T cells were transfected with either 2 μg of pCAGGS- vMIP-I or 2 μg of pCAGGS-vMIP-II plasmids. Forty-eight hours after transfection, the cells were harvested and expression of vMIP-I or vMIP-II was tested by Western blot analysis using the anti-vMIP-I or -vMIP-II MAb, respectively. Actin was also probed with anti-actin monoclonal Ab as a loading control.

obtained from the American Type Culture Collection (ATCC) (Manassas, VA). These cells were grown in RPMI 1640 (Nakalai Tesque, Inc., Kyoto, Japan) supplemented with 10 IU/ml penicillin G, 10 μg/ml streptomycin, 10% heat-inactivated fetal bovine serum (FBS) (HyClone, Logan, UT) in a 5% CO_2 atmosphere. In addition, 293 T and 293/EBNA (Clontech) cells were grown in Dulbecco's modified Eagle's medium (DMEM) (Nakalai Tesque, Inc.) supplemented with 10 IU/ml penicillin G, and 10 μg/ml streptomycin, 10% FBS, and 200 mM L-glutamine.

Plasmids

In order to express vMIP-I and vMIP-II, the ORFs were cloned into the pCAGGS eukaryotic expression vector, and pCAGGS-vMIP-I and pCAGGS-vMIP-II were established. The plasmid vector, pCAGGS was kindly provided by Dr. J. Miyazaki of Osaka University (Niwa et al., 1991). Briefly, fragments including vMIP-I and vMIP-II ORFs were amplified by PCR using the following primer sets: vMIP-I-Met (5′-CGGTACCGAATTCTCCAGATGGCC-3′) and vMIP-I-Ter (5′-ACTCGAGAATTCTACTTGTCATCGTCGTCCTTGTAGTCGGAAGCTATGGCAGGCAG-3′); and vMIP-II-Met (5′-AGGTACCGAATTCAGTTATGGACACCAAGGGC-3′) and vMIP-II-Ter (5′-ACTCGAGAATTCTACTTGTCATCGTCGTCCTTGTAGTCGGAGCGAGCAGTGACTGG-3′). The PCR products were cloned into pCR2.1 (Invitrogen) and sequenced. After digestion with *Eco*RI, the fragments were ligated into the *Eco*RI site of the pCAGGS vector. Then, the DNA fragments encoding vMIP-I and vMIP-II were liberated by *Eco*RI, and were inserted into pCAGGS to generate the expression vectors pCAGGS-vMIP-I and -vMIP-II, respectively. vMIP-I (pGEX-vMIP-I) and vMIP-II (pGEX-vMIP-II) were also generated using PCR-based technology using BCBL-1 genomic DNA as a templete. The coding region, without a signal peptide, was amplified with vMIP-I-Eco (CAGAATTCGCGGGGTCACTCGTGTCG-3′), vMIP-I-Sal (CTGTCGACCGTCTAAGCTATGGCAGG-3′), vMIP-II-Eco (5′-CGGAATTCGCGTCCTGGCATAGACCG-3′), and vMIP-II-Sal (5′-GGGTCGACATTCTTCAGCGAGCAGTG-3′). The amplified vMIP-I and the vMIP-II fragments were digested with *Eco*RI and *Sal*I and inserted downstream of the GST coding of pGEX-5X-1 (GE Healthcare, Uppsala, Sweden) at the *Eco*RI and *Sal*I sites to construct pGEX-vMIP-I and pGEX-vMIP-II. To express a full-length and the deletion mutants of the GST-vMIP-I and GST-vMIP-II fusion protein, the genes for GvM1-Full, GvM1-D1, GvM1-D2,

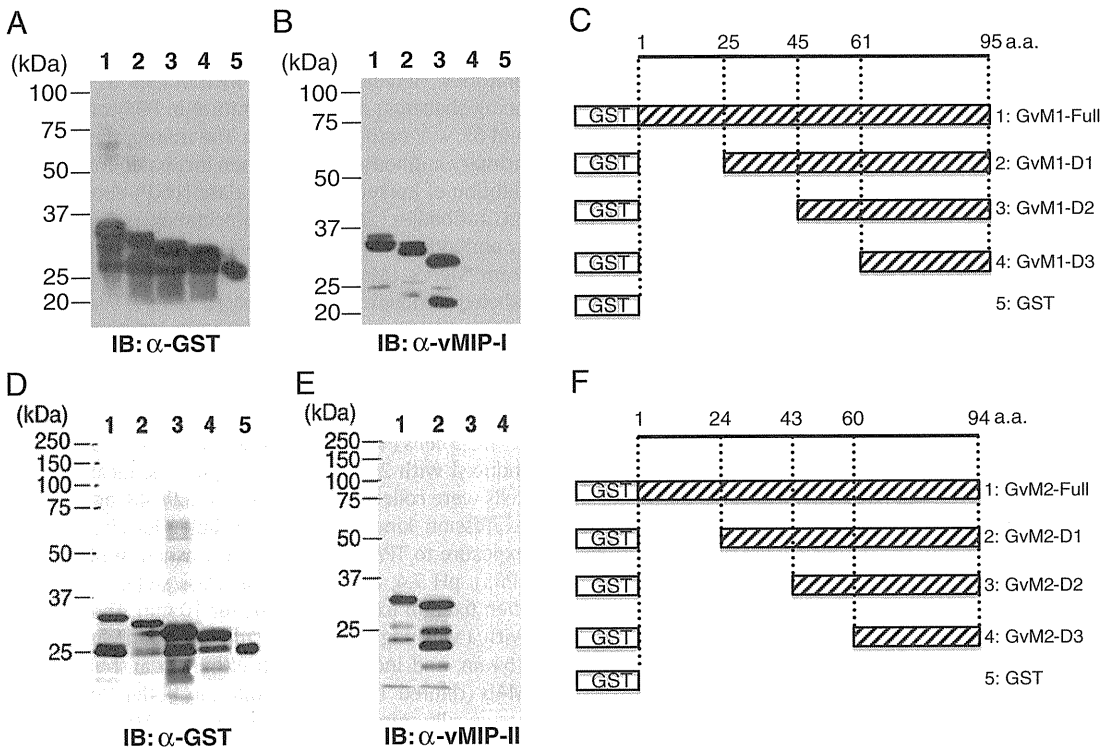

Fig. 2. Epitope mapping of the anti-vMIP-I and the anti-vMIP-II MAbs. To map the regions of vMIP-I and vMIP-II recognized by the anti-vMIP-I and anti-vMIP-II antibody, a series of GST-vMIP-I and GST-vMIP-II fusion proteins containing the individual regions of vMIP-I and vMIP-II were constructed as described in Fig. 2C and F, and the proteins were expressed in *E. coli*. The lysates of the fusion proteins, vMIP-I and vMIP-II, and its deletion mutants were immunoblotted with an anti-GST antibody (A and D) and an anti-vMIP-I (B) and an anti-vMIP-II antibody (E) to detect GST-vMIP-I or GST-vMIP-II fusion proteins. Lane 1, GvM1-Full; lane 2, GvM1-D1; lane 3, GvM1-D2; lane 4, GvM1-D3; lane 5, GvM1-D4; lan3 6, GST in Fig. 2A and B. Lane 1, GvM2-Full; lane 2, GvM2-D1; lane 3, GvM2-D2; lane 4, GvM2-D3; lane 5, GST (in D only) in Fig. 2D and E. Summary of GST-vMIP-I (C) and GST-vMIP-II (F) deletion mutants. Individual regions of vMIP-I and vMIP-II were cloned in-frame into the pGEX-5X-1 vector to generate GST-vMIP-I and GST-vMIP-II fusion proteins, respectively. The boxes at left indicate GST, and the white boxes with slashed lines indicate individual domains of vMIP-I and vMIP-II. 1, GvM1-Full(1-95a.a.); 2, GvM1-D1(25-95a.a.); 3, GvM1-D2(45-95a.a.); 4, GvM1-D3(61-95a.a.) in Fig. 2C, and 1, GvM2-Full(1-94a.a.); 2, GvM2-D1(24-94a.a.); 3, GvM2-D2(43-94a.a.); 4, GvM2-D3(60-94a.a.) in Fig. 2F.

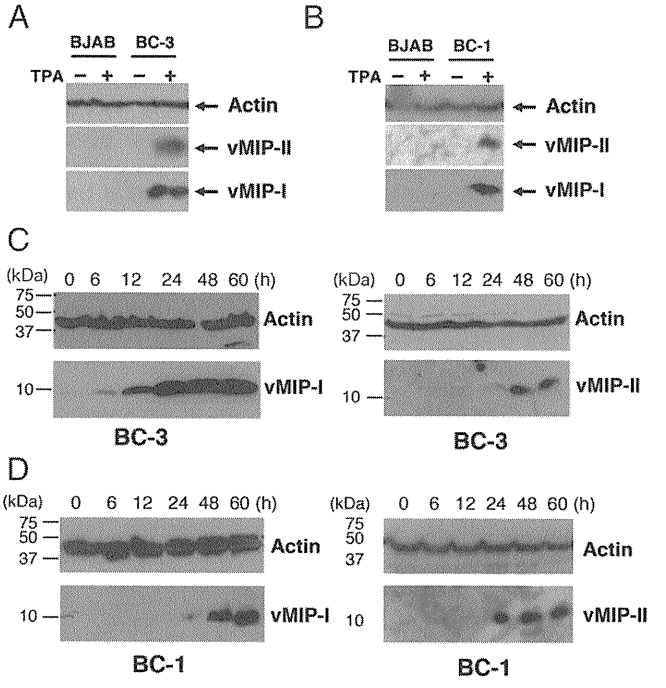

Fig. 3. Detection of vMIP-I and vMIP-II gene products in a KSHV-infected PEL cell line. BC-1 and BC-3 cells were treated with TPA for the indicated number of hours, and the whole-cell extract was prepared after the indicated time post-induction. vMIP-I and vMIP-II were detected by Western blotting and IFA with anti-vMIP-I and -vMIP-II antibodies. Western blot analysis of protein extracted from BC-3 and BJAB cells (A), and BC-1 and BJAB cells (B) with either the anti-vMIP-I or the anti-vMIP-II MAb. Arrows indicate actin, vMIP-I, and vMIP-II proteins. As expected, the estimated sizes of the vMIP-I and vMIP-II proteins, based on comparisons with the migration of molecular size markers, was around 10 kDa. Expression kinetics of vMIP-I (left panel) and vMIP-II (right panel) in TPA-treated BC-3 (C) and BC-1 (D) cells by Western blot analysis. BC-1 and BC-3 cells were harvested after 6, 12, 24, 48, and 60 h post-induction. The lysate was subjected to Western blot analysis as in (A).

GvM1-D3, GvM2-Full, GvM2-D1, GvM2-D2, and GvM2-D3 genes were generated by PCR using the following primer sets: vMIP-I-1F (5′-ATGAATTCCAGATGGCCCCCGTCCAC-3′) and vMIP-I-5R (5′-CCGTGTCGACCGTCTAAGCTATGGCAGGCAGC-3′); vMIP-I-2F (5′-ATGAATTCGCGGGGTCACTCGTGTCG-3′) and vMIP-I-5R; vMIP-I-3F (5′-ATGAATTCCCGCCCGTCCAAATTC-3′) and vMIP-I-5R; vMIP-I-4F (5′-ATGAATTCCCAAAACCCGGAGTTATTTTGC-3′) and vMIP-I-5R; vMIP-II-1F (5′-CGGAATTCGTTATGGACACCAAGGGC-3′) and vMIP-II-5R (5′-GGCAGTCGACTCTTCAGCGAGCAGTGACTG-3′); vMIP-II-2F (5′-GGGAATTCCTGGGAGCGTCCTGGCATAGAC-3′) and vMIP-II-5R; vMIP-II-3F (5′- AAGAATTCTTACCACAGGTGCTTCTGTCC-3′) and vMIP-II-5R; and vMIP-II-4F (5′-TGGAATTCAAGCCGGGTGTGATATTTTTG-3′) and vMIP-II-5R. The PCR products were cloned into pCR2.1 (Invitrogen, Carlsbad, CA) and confirmed by sequencing. The products were digested with the *Eco*RI and *Sal*I restriction enzymes and were cloned into pGEX-5X-1 (GE Healthcare). The PCR conditions for all products were as follows: 25 cycles of 94 °C for 1 min, 55 °C for 1 min, and 72 °C for 2 min in a TP480 PCR thermal cycler (Takara Shuzo, Kyoto, Japan).

Immunization and generation of monoclonal Abs against vMIP-I and vMIP-II

In mice, anti-vMIP-I and -vMIP-II antibodies were raised against the GST-vMIP-I and GST-vMIP-II fusion protein, respectively. These GST fusion proteins were purified on a glutathione-Sepharose 4B column (GE Healthcare), and the GST-vMIP-I and the GST-vMIP-II fusion proteins were conjugated to keyhole limpet hemocyanin KLH (Calbiochem. Co., La Jolla, CA). Mice were initially immunized with 250 μg each of the purified GST-vMIP-I or -II fusion protein in Freund's complete adjuvant administered to the peritoneal cavity, and 200 μg of the antigen in Freund's incomplete adjuvant were injected again 14 and 28 days after the first injection. The mice were exsanguinated 7 days after the last injection. To generate MAbs against vMIP-I and vMIP-II, hybridomas were established by fusing splenocytes from the hyperimmune mice using a nonproducing myeloma cell line, Sp-2/0-Ag14 (ATCC, Manassas, VA). After selection in medium containing hypoxanthine-aminopterin-thymidine, cells secreting MAbs were screened by immunofluorescence assays (IFA). The TPA-induced and -uninduced BCBL-1 cells were fixed in acetone and exposed to supernatants of the hybrid cells. Clones secreting antibodies reactive with TPA-stimulated BCBL-1 cells were expanded and isolated by limiting dilutions.

Transfection analysis of vMIP-I and vMIP-II

To express the vMIP-I and vMIP-II proteins, 293/EBNA cells were transfected with pCAGGS-vMIP-I and -vMIP-II plasmids using TransIT-LT1 (Mirus Bio LLC, Madison, WI). The transfected cells were incubated for 48 h in DMEM supplemented with 10% FCS. The cells were harvested and lysed with lysis buffer (0.05 M Tris-HCl [pH 8.0], 0.15 M NaCl, 0.5% sodium deoxycholate, 1% Triton X-100, 0.1% sodium-dodecyl sulfate [SDS]). The cell lysate was fractionated by electrophoresis on 16% polyacrylamide gel as described below.

Antibodies and Western blotting

The expression of vMIP-I and vMIP-II in BC-3 cells stimulated with TPA was determined with MAbs against vMIP-I and vMIP-II, respectively, as noted above. The concentration of proteins extracted from BC-3 cells was normalized using a BCA Protein Assay Kit (Thermo Fisher Scientific Inc., Rockford, IL). The samples were subjected to SDS-15% polyacrylamide gel electrophoresis under reducing conditions, and were electrophoretically transferred to PVDF membranes (Bio-Rad Laboratories, Hercules, CA). The membranes were blocked for 1 h while being shaken at room temperature in PBS containing 0.05% Tween 20 and 5% w/v nonfat skim milk. The membranes were incubated with a primary antibody and were then incubated for 1 h with an appropriate dilution of horseradish peroxidase (HRP)-conjugated goat anti-mouse IgG antibodies (Santa Cruz Biotechnologies, Santa Cruz, CA). The primary antibody against actin, anti-actin (Ab-1) mouse MAb, was purchased from Merck (Merck KGaA, Darmstadt, Germany). The bound HRP-labeled antibodies were detected with a West Pico substrate kit for horseradish peroxidase (Thermo Fisher Scientific Inc).

IFA

BC-3 cells (10^7 cells) in RPMI 1640 medium with supplements were induced with 25 ng/ml TPA (Sigma Chemical Co., St. Louis, MO). The cells were collected after 0, 4, 8, 12, 24, 48, and 60 h for analysis of the expression kinetics, and for cellular localization analysis 48 h after exposure to TPA. The cells were washed in phosphate-buffered saline (PBS), pH 7.4, and spotted on glass slides. The spots were air-dried, then fixed in ice-cold acetone for 10 min. The cells were then washed with a washing buffer (PBS supplemented with 0.1% Triton X-100) for 15 min, and incubated with either an anti-vMIP-I or an anti-vMIP-II MAb (diluted 1:100 in IFA dilution buffer [PBS containing 2% bovine serum albumin, 0.2% Tween-20, and 0.05% NaN_3]) for 1 h at 37 °C. Then, the slides were washed with the washing buffer, and incubated for 1 h at room temperature with a pre-standardized diluted fluorescein isothiocyanate (FITC)-conjugated goat anti-mouse IgG (Tago Immunologicals, Camarillo, CA). The slides were washed and stained with 4′, 6′-diamidino-2-phenylindole (DAPI) to detect nuclei and were mounted with 50% (v/v) glycerol in PBS. For formalin-fixed paraffin-embedded tissues, antigen retrievals were performed on the de-paraffined sections using citrate buffer. Alexa 488 or 568-conjugated

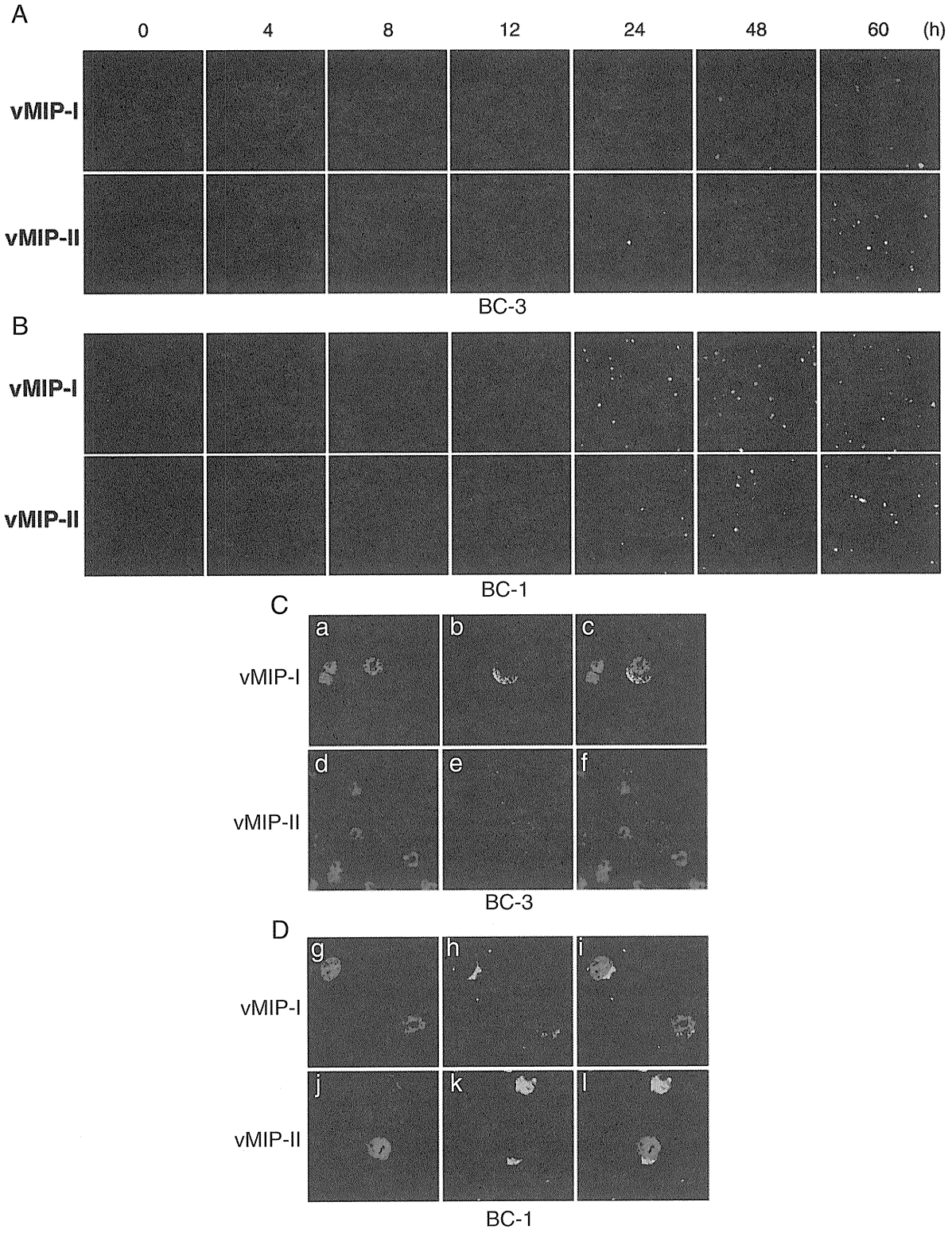

Fig. 4. Expression of vMIP-I and vMIP-II in BC-3 and BC-1 cells by IFA. After 4, 8, 12, 24, 48, and 60 h, BC-3 (A) and BC-1 (B) cells were labeled either with the anti-vMIP-I (upper) or the anti-vMIP-II (lower) MAb followed by goat anti-mouse FITC-conjugated Abs. FITC photomicrographs showing anti-vMIP-I and anti-vMIP-II immunoreactivity in BC-3 and BC-1 cells treated with TPA. (C) Cellular localization of vMIP-I and vMIP-II in BC-3 (C) and BC-1 (D) cells. The cells were stained with DAPI (a, d, g and j), and the localization of vMIP-I and vMIP-II was visualized by IFA with anti-vMIP-I or -vMIP-II MAbs (b, e, h and k); panel a and b, d and e, g and h, and j and k were merged (c, f, i and l). Fluorescence photomicrographs revealed anti-vMIP-I and -vMIP-II immunoreactivity using FITC-conjugated anti-mouse IgG MAb.

anti-mouse or rabbit antibodies (Invitrogen) were used as the secondary antibodies. Confocal microscopic analysis was performed (FV-1000, Olympus, Tokyo, Japan), and the contrast was adjusted before the images were exported as TIFF files to Adobe Photoshop.

Immunohistochemistry

Formalin-fixed paraffin-embedded tissues from KS and MCD patients, and those from an animal model of KSHV-associated solid lymphoma

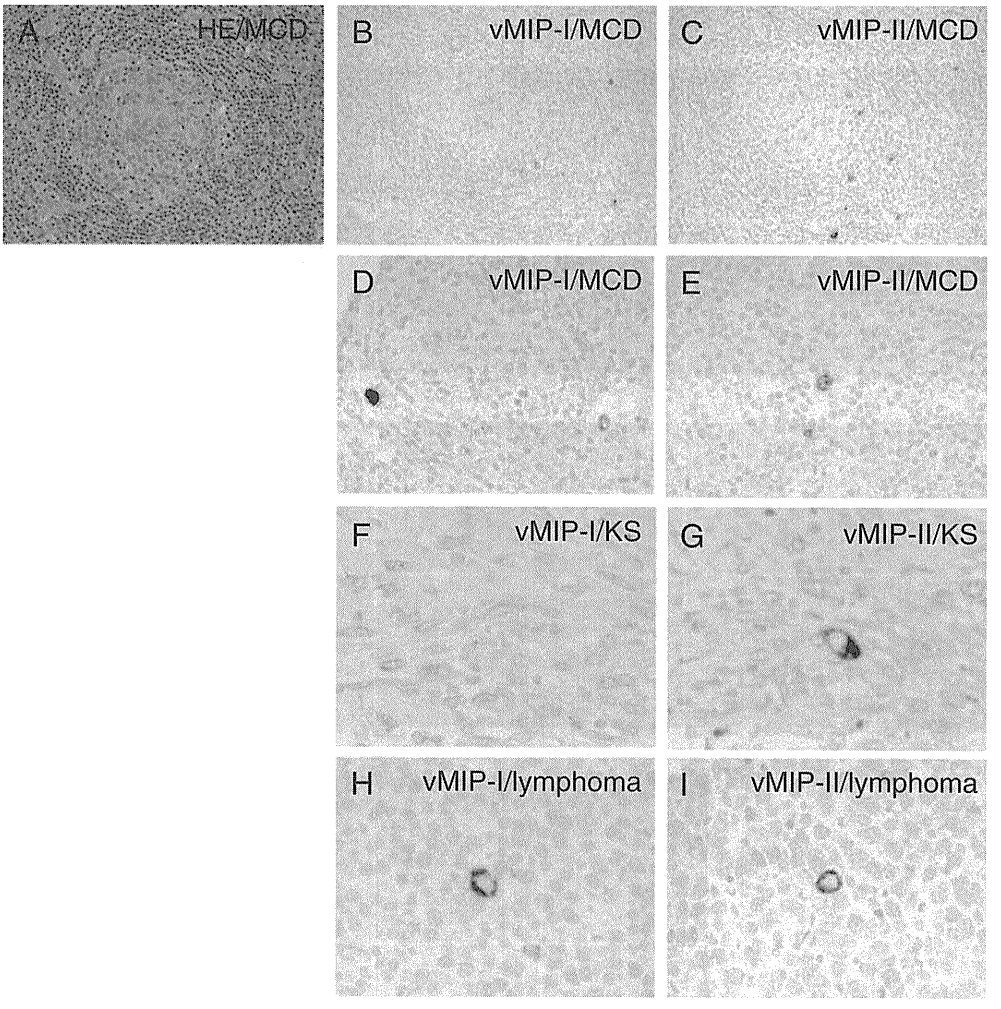

Fig. 5. Expression of vMIP proteins in KSHV-associated diseases. (A–C) Hematoxylin and eosin staining and immunohistochemistry for vMIPs in serial sections of a tissue sample from a patient with MCD. Brown stains indicate positive signals. The nucleus was counter-stained by hematoxylin. (D and E) Higher magnification view of vMIPs expression in an MCD case. Some large lymphocytes in the mantle zone were stained. (F and G) vMIP-I and vMIP-II expression in a KS sample. (H and I) Expression of vMIPs in an animal model of KSHV-associated lymphoma in SCID mice.

were sectioned and stained with hematoxylin and eosin (H&E). Immunohistochemistry of the serial sections was performed with either the anti-vMIP-I or -II MAb. For the second- and third- phase reagents used for immunostaining, a CSAII kit (DAKO, Copenhagen, Denmark) was used. An animal model of KSHV-associated solid lymphoma, which was established as described previously (Katano et al., 2000b), was also subjected to immunohistochemical analysis. Briefly, TY-1 cells were inoculated into the subcutaneous tissue of mice with severe combined immunodeficiency (SCID). One month after inoculation, lymphomas appeared in the subcutaneous region at the inoculation site. Lymphoma cells contained the KSHV genome, and expressed various viral proteins of KSHV (Katano et al., 2000b).

Table 1
Expression of vMIP-I and vMIP-II in MCD and KS tissue samples.

	KSHV proteins, (+)/total	
Cases	vMIP-I	vMIP-II
MCD	(3)/3	(3)/3
KS	(0)/5	(2)/8

Chemotaxis assays

Chemotaxis assays were performed as described previously (Nakano et al., 2003). Briefly, THP-1 cells were washed twice with chemotaxis buffer, 0.5% bovine serum albumin, 20 mM HEPES, pH 7.4, in RPMI 1640. Migration of cells was assessed in a cell culture chamber (Costar, Cambridge, MA), with the upper and lower compartments separated by a 3 μm pore size polycarbonate filter (???). The lower compartment of the chamber was filled with dilutions of vMIP-I, vMIP-II (R&D Systems, Minneapolis, MN) or with PBS alone, and/or with each 10 μg/ml anti-vMIP-I or -vMIP-II MAbs at a volume of 600 μl. The upper compartment contained 100 μl of THP-1 cell suspensions in chemotaxis buffer (10^5 cells/well). The chambers were then incubated for 4 hours at 37 °C, 5% CO_2, and spun at 300 x g, 4 °C, for 5 min. Finally, the cells from the lower compartment were counted.

Results

Specificity of the anti-vMIP-I MAb and the anti-vMIP-II MAb

In order to check specificity of the MAbs, we transfected vMIP-I and vMIP-II expression vectors (pCAGGS-vMIP-I, and -II) into 293/EBNA

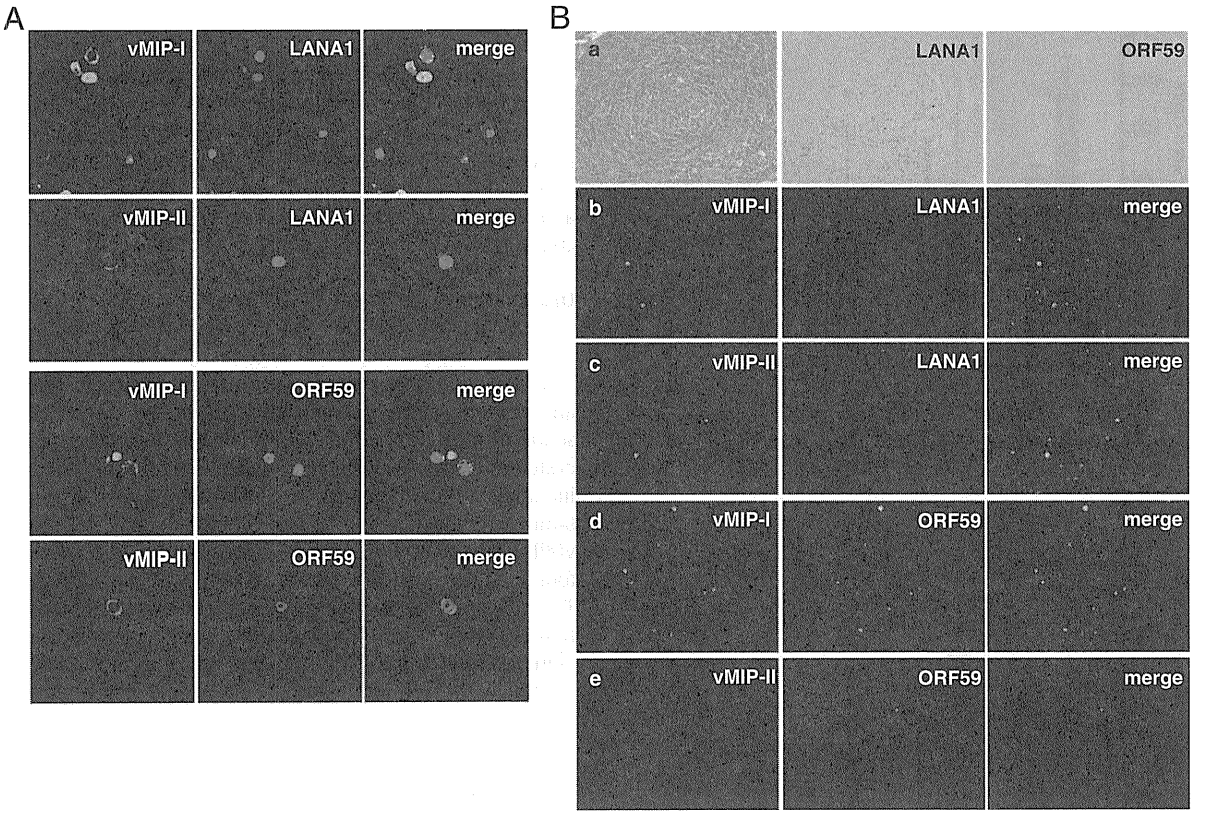

Fig. 6. (A) Expression of vMIPs. LANA1 and ORF59 in the animal model of KSHV-associated solid lymphoma by confocal microscopy. vMIPs were labeled with Alexa 488 (green). LANA1 (upper panels) and ORF59 (lower panels) were labeled with Alexa 568 (red). (B) Expression of vMIPs in MCD. (a) HE staining and immunohistochemistry of LANA1 and ORF59. (b–e) Immunofluorescence assay on MCD lesion. A germinal center is shown in the center of each panel. This case is KSHV-positive large B cell lymphoma arising in MCD (for interpretation of the color references in this article, the reader is referred to the online version).

cells, respectively. The total lysate of the transfected cells was subjected to Western blot analysis. vMIP-I and vMIP-II proteins were detected with anti-vMIP-I or vMIP-II MAbs, respectively (Fig. 1). These antibodies did not show cross-reactivity each other.

Epitope mapping of the anti-vMIP-I and anti-vMIP-II MAbs

We established hybridoma clones secreting MAbs against vMIP-I and vMIP-II, respectively. To map the regions of vMIP-I and vMIP-II where anti-vMIP-I and anti-vMIP-II antibody reacted, a series of GST-fused vMIP-I and vMIP-II deleted proteins were constructed as described in Fig. 2C and F, and used for Western blot analysis with an anti-GST antibody (Santa Cruz Biotechnology Inc), (Fig. 1A, D) and the anti-vMIP-I or the anti-vMIP-II (Fig. 1B, E) antibody, respectively. The results showed that all GST-vMIP-I and GST-vMIP-II fusion proteins interacted with the anti-GST antibody (Fig. 2A, D) and showed that GvM1-Full, GvM1-D1, and GvM1-D2 reacted with the anti-vMIP-I antibody, whereas GvM1-D3 did not (Fig. 1B), and GvM2-Full and GvM2-D1 reacted with the anti-vMIP-II antibody, whereas GvM2-D2, and GvM2-D3 did not (Fig. 2E). Thus, these results demonstrated that an anti-vMIP-I MAbs was successfully generated and suggest that the amino acid residues 61 to 95 of vMIP-I could be a major epitope reacted with the anti-vMIP-I antibody. On the other hand, the amino acid residues 24 to 42 of vMIP-II could be an epitope reacted with the anti-vMIP-II antibody.

Expression of vMIP-I and vMIP-II in the KSHV-infected PEL cell line

We tested vMIP-I and vMIP-II expression in KSHV and Epstein Barr virus (EBV) dually infected PEL cell lines (BC-1), KSHV infected PEL cell lines (BC-3) and in non-infected Burkitt's lymphoma cell line (BJAB), and detected them in TPA-stimulated BC-3 and BC-1 cells with developed antibodies, but not in BJAB cells non-stimulated BC-3 or BC-1 cells (Fig. 2A, B). In a KSHV infected PEL cells, BC-1 and BC-3, vMIP-I and vMIP-II were detected around at 10 kDa, which matches the size deduced from amino acids length (Fig. 3C, D). Actually, vMIP-I was detected from 6 hours post induction and vMIP-II was at 24 hours in BC-3 cells (Fig. 3C), and vMIP-I and vMIP-II were detected at 24 h in BC-1 cells (Fig. 3D). In the immunofluorescence microscopy, the number of vMIP-II expressing cells seemed to be more than that of vMIP-I in BC-3 cells (Fig. 4A, B). In order to analyze the cellular localization of vMIP-I and vMIP-II protein, BC-3 and BC-1 cells stimulated with TPA were doubly labeled with DAPI (Fig. 4C, a, d and D, g, j), and either the anti-vMIP-I MAb (Fig. 4C, b and D, h) or the anti-vMIP-II MAb (Fig. 4C, e and D, k). Merged images were shown in Fig. 4C, c, f, and D, i, l). The vMIP-I and the vMIP-II clearly showed cytoplasm and possibly membranes in TPA-induced BC-3 and BC-1 cells (Fig. 4C, b, e, and D, h, k).

Expression of vMIPs in KSHV-associated diseases

To know the expression of vMIPs in KSHV-associated diseases, immunohistochemistry for vMIPs was performed on pathological samples of eight KS cases, three MCD cases, and the animal model of KSHV-associated solid lymphoma (Fig. 5). Immunohistochemistry demonstrated that vMIP-I and vMIP-II were detected in some cells in the mantle zone of germinal center and the interfollicular zone in KSHV-positive MCD samples (Fig. 5A to E). Both vMIP-I and vMIP-II were detected predominantly in the cytoplasm of large lymphocytes. The numbers of positive cells varied among three MCD cases examined. On the other

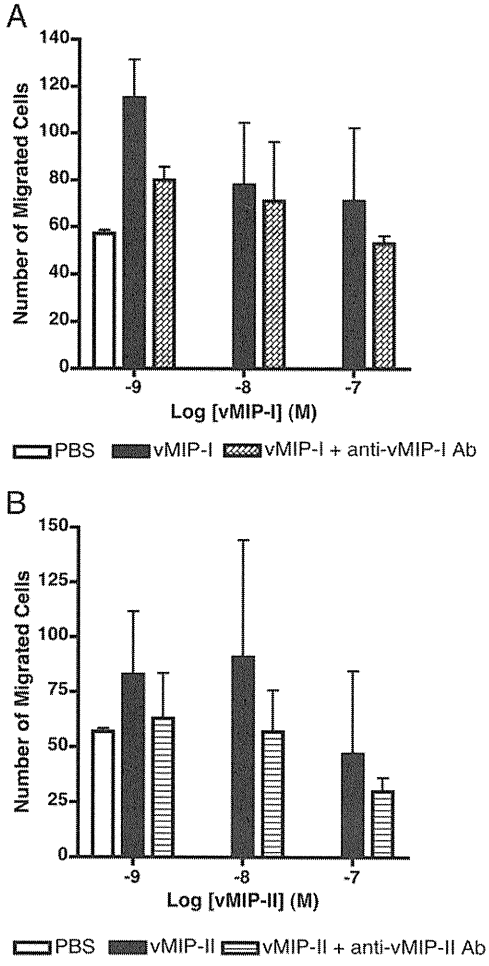

Fig. 7. Neutralizing activity of anti-vMIP-I and -vMIP-II MAbs. THP-1 cell migration in response to increased concentrations of vMIP-I and vMIP-II (1, 10, 100 nM), and the neutralizing activity of 10 μg/ml anti-vMIP-I and -vMIP-II MAbs against vMIP-I and vMIP-II were measured, as outlined in Materials and Methods, by using the transwell migration assay system. Various doses of vMIP-I and vMIP-II were tested for their ability to induce the chemotaxis of THP-1 cells. The data presented are from one experiment, and are representative of the triplicate experiments performed. The error bars indicate the standard deviations of three independent experiments.

hand, any positive signal of vMIP-I was not observed in all KS cases (Fig. 5F, G). vMIP-II was rarely detected in the cytoplasm of spindle cells in two KS cases at the nodular stage out of eight KS cases. In the samples of animal model of KSHV-associated solid lymphoma, both vMIP-I and vMIP-II were detected in the cytoplasm of a part of lymphoma cells (Fig. 5H, I). These data showed that vMIP-I and vMIP-II were expressed in cells in MCD and KSHV-associated lymphoma, but vMIP-II was rarely in KS (Table 1). To know the association of vMIPs expression with expression of other KSHV-encoded proteins, we examined immunofluorescence assay on KSHV-associated diseases. Since, all KSHV-infected cells express LANA1, vMIPs-positive cells were positive for LANA1. However, expression pattern of LANA1 showed diffuse nuclear staining in vMIPs-positive cells in the animal model of KSHV-associated solid lymphoma (Fig. 6A). Confocal microscopy revealed that vMIP-I stain showed usually cytoplasmic pattern, but rarely diffuse nuclear staining pattern *in vivo*. Almost all cells with vMIPs expression were also positive for ORF59 protein, a lytic protein of KSHV. IFA also demonstrated that vMIPs-positive cells expressed LANA1 at various levels in MCD clinical samples (Fig. 6B, a to c). A large portion of vMIPs-positive cells also expressed ORF59 protein in MCD (Fig. 6B, d, e). These data suggest that vMIPs are expressed by cells with KSHV-lytic infection in KSHV-associated MCD and lymphoma.

Neutralization of vMIP-I and vMIP-II by anti-vMIP-I and anti-vMIP-II MAbs

We examined whether the anti-vMIP-I and anti-vMIP-II MAbs could neutralize the chemoattractant of vMIP-I and vMIP-II to induce the migration of THP-1 cells. As expected, vMIP-I and vMIP-II induced migration of THP-1 cells (Fig. 7A, B), but not with PBS alone. However, anti-vMIP-I and anti-vMIP-II MAbs inhibited respective vMIP-I and vMIP-II-induced cell migration of THP-1 cells at 10 μg/ml final concentration.

Discussions

It was known that KSHV encodes three chemokine genes of the so-called viral macrophage inflammatory proteins: *vMIP-I*, *vMIP-II*, and *vMIP-III* in the genome. Analysis of the translated amino acid sequence indicate that the vMIP-I and vMIP-II gene have four conserved cysteines capable of forming two essential disulfide bonds (first cysteine and third cysteine, and second cysteine and fourth cysteine). The family of chemokines comprises CC, CXC, C, and CX_3C subfamilies. The vMIP-I and vMIP-II have four cysteines, the first two of which are found in the sequence of CC, which correspond to the CC profile. These gene products were expressed in the phase of KSHV lytic infection (Moore et al., 1996; Sun et al., 1999). Both vMIP-I and vMIP-II were expressed in a KSHV-infected cell lines, BC-3, which had been treated with TPA. Mono-specific polyclonal Abs against vMIP-I and vMIP-II have been described in previous studies that investigated the localization of vMIPs in PEL cells (Nakano et al., 2003). In the present study, we developed the respective MAbs that reacted either with KSHV vMIP-I or vMIP-II. We first applied these MAbs against KSHV vMIP-I and vMIP-II to detect KSHV-infected BC-3 and BC-1 cells by Western blotting and immunofluorescence assay. The Western blot analysis revealed that both the anti-vMIP-I and the anti-vMIP-II MAbs reacted to the 10-kDa proteins considered specific to the respective vMIP protein. The anti-vMIP-I MAb was shown to be reactive with the epitopes in the middle of the protein (sequence, PPVQILKEWYPTSPAC), and the epitope of the anti-vMIP-II MAb was shown to be reactive at the N-terminal end (sequence, LGASWHRPDKCCLGYQKRP). Further immunofluorescence analysis of the cellular localization of both vMIP-I and vMIP-II with anti-vMIP-I and anti-vMIP-II MAb showed a cytoplasmic pattern of expression in BC-3 and BC-1 cells. As the results indicated that these gene products were expressed in the cytoplasm, it might be located at the KSHV-infected BC-3 or BC-1 cells membrane prior to secretion. An investigation of the antigenic specificities of MAbs against KSHV vMIP-I and vMIP-II in MCD and KS patients has not yet been reported. Here, immunohistochemical analysis detected only vMIP-II in samples from both KS and MCD patients, but vMIP-I was not detected in KS cases: however, both vMIP-I and vMIP-II proteins were expressed in some cells in the interfollicular zone of MCD tissues. Lytic proteins of the KSHV such as K8, RTA, and ORF59 have been detected in large lymphocytes in the mantle zone of MCD cases (Dupin et al., 1999; Katano et al., 2000a). The expression of vMIPs showed a similar pattern to that of the lytic proteins in MCD tissues. In contrast, lytic protein expression, including that of vMIPs, was rare in the KS lesions (Abe et al., 2006). In the present study, we demonstrated that vMIPs were expressed in the cells expressing ORF59 protein. Thus, our data clearly indicated that the expression of vMIPs is associated with lytic infection in individual cells affected by KSHV-associated diseases. Human monocytic cell line THP-1 respond to various chemokines suggesting that they express receptors for these chemokines (Wang et al., 1993). Previous study, vMIP-I and vMIP-II were shown chemotaxis in THP-1 cells (Nakano et al., 2003). It has been reported that vMIP-I acts as a specific agonist for CC chemokine receptor 8 (CCR8) (Dairaghi et al., 1999; Endres et al., 1999) and vMIP-II shows a Ca^{2+} flux as a specific agonist for CCR3 (Boshoff et al., 1997). Our data showed anti-vMIP-I and anti-vMIP-II MAbs were able to neutralize vMIP-I- and vMIP-II-mediated chemotaxis in THP-1 cells. However, neutralizing activities

of anti-vMIP-I MAb was apparently low, even the addition of 10 μg/ml MAbs. These findings support the assumption that anti-vMIP-I and –vMIP-II MAbs-blocked chemotaxis in THP-1 cells act through binding to the certain amino acid residue of vMIP-I and vMIP-II.

In summary, MAbs developed specifically for this series were used to detect vMIP-I and vMIP-II in MCD and KS tissues, which may account for certain clinical features of MCD and KS. To gain a better understanding of these important viral genes, additional studies will be needed that focus on revealing vMIP-I and vMIP-II expression profiles during lytic infection. Taken together, these studies provide an insight into the pathogenesis of the contribution of vMIP-I and vMIP-II to the lytic induction of KSHV. These MAbs could serve as useful tools to clarify the pathogenesis of KSHV-related diseases.

Acknowledgments

This study was supported by a grant for Research on Publicly Essential Drugs and Medical Devices from the Japan Health Sciences Foundation (SAA4832), Health and Labor Sciences Research Grants (to HK, No. H23-AIDS-Ippan-002) from the Ministry of Health and by a grant from PRESTO of the Japan Science and Technology Corporation (200154023).

References

Abe, Y., Matsubara, D., Gatanaga, H., Oka, S., Kimura, S., Sasao, Y., Saitoh, K., Fujii, T., Sato, Y., Sata, T., Katano, H., 2006. Distinct expression of Kaposi's sarcoma-associated herpesvirus-encoded proteins in Kaposi's sarcoma and multicentric Castleman's disease. Pathol. Int. 56, 617–624.

Arvanitakis, L., Mesri, E.A., Nador, R.G., Said, J.W., Asch, A.S., Knowles, D.M., Cesarman, E., 1996. Establishment and characterization of a primary effusion (body cavity-based) lymphoma cell line (BC-3) harboring kaposi's sarcoma-associated herpesvirus (KSHV/HHV-8) in the absence of Epstein-Barr virus. Blood 88, 2648–2654.

Benelli, R., Barbero, A., Buffa, A., Aluigi, M.G., Masiello, L., Morbidelli, L., Ziche, M., Albini, A., Noonan, D., 2000. Distinct chemotactic and angiogenic activities of peptides derived from Kaposi's sarcoma virus encoded chemokines. Int. J. Oncol. 17, 75–81.

Boshoff, C., Endo, Y., Collins, P.D., Takeuchi, Y., Reeves, J.D., Schweickart, V.L., Siani, M.A., Sasaki, T., Williams, T.J., Gray, P.W., Moore, P.S., Chang, Y., Weiss, R.A., 1997. Angiogenic and HIV-inhibitory functions of KSHV-encoded chemokines. Science 278, 290–294.

Cesarman, E., Chang, Y., Moore, P.S., Said, J.W., Knowles, D.M., 1995. Kaposi's sarcoma-associated herpesvirus-like DNA sequences in AIDS-related body-cavity-based lymphomas. N. Engl. J. Med. 332, 1186–1191.

Chang, Y., Cesarman, E., Pessin, M.S., Lee, F., Culpepper, J., Knowles, D.M., Moore, P.S., 1994. Identification of herpesvirus-like DNA sequences in AIDS-associated Kaposi's sarcoma. Science 266, 1865–1869.

Chen, S., Bacon, K.B., Li, L., Garcia, G.E., Xia, Y., Lo, D., Thompson, D.A., Siani, M.A., Yamamoto, T., Harrison, J.K., Feng, L., 1998. In vivo inhibition of CC and CX3C chemokine-induced leukocyte infiltration and attenuation of glomerulonephritis in Wistar–Kyoto (WKY) rats by vMIP-II. J. Exp. Med. 188, 193–198.

Dairaghi, D.J., Fan, R.A., McMaster, B.E., Hanley, M.R., Schall, T.J., 1999. HHV8-encoded vMIP-I selectively engages chemokine receptor CCR8. Agonist and antagonist profiles of viral chemokines. Biol. Chem. 274, 21569–21574.

Dupin, N., Fisher, C., Kellam, P., Ariad, S., Tulliez, M., Franck, N., van Marck, E., Salmon, D., Gorin, I., Escande, J.P., Weiss, R.A., Alitalo, K., Boshoff, C., 1999. Distribution of human herpesvirus-8 latently infected cells in Kaposi's sarcoma, multicentric Castleman's disease, and primary effusion lymphoma. Proc. Natl. Acad. Sci. U. S. A. 96, 4546–4551.

Endres, M.J., Garlisi, C.G., Xiao, H., Shan, L., Hedrick, J.A., 1999. The Kaposi's sarcoma-related herpesvirus (KSHV)-encoded chemokine vMIP-I is a specific agonist for the CC chemokine receptor (CCR)8. J. Exp. Med. 189, 1993–1998.

Katano, H., Sato, Y., Kurata, T., Mori, S., Sata, T., 2000a. Expression and localization of human herpesvirus 8-encoded proteins in primary effusion lymphoma, Kaposi's sarcoma, and multicentric Castleman's disease. Virology 269, 335–344.

Katano, H., Suda, T., Morishita, Y., Yamamoto, K., Hoshino, Y., Nakamura, K., Tachikawa, N., Sata, T., Hamaguchi, H., Iwamoto, A., Mori, S., 2000b. Human herpesvirus 8-associated solid lymphomas that occur in AIDS patients take anaplastic large cell morphology. Mod. Pathol. 13, 77–85.

Kledal, T.N., Rosenkilde, M.M., Coulin, F., Simmons, G., Johnsen, A.H., Alouani, S., Power, C.A., Luttichau, H.R., Gerstoft, J., Clapham, P.R., Clark-Lewis, I., Wells, T.N., Schwartz, T.W., 1997. A broad-spectrum chemokine antagonist encoded by Kaposi's sarcoma-associated herpesvirus. Science 277, 1656–1659.

Miller, G., Heston, L., Grogan, E., Gradoville, L., Rigsby, M., Sun, R., Shedd, D., Kushnaryov, V.M., Grossberg, S., Chang, Y., 1997. Selective switch between latency and lytic replication of Kaposi's sarcoma herpesvirus and Epstein-Barr virus in dually infected body cavity lymphoma cells. J. Virol. 71, 314–324.

Moore, P.S., Boshoff, C., Weiss, R.A., Chang, Y., 1996. Molecular mimicry of human cytokine and cytokine response pathway genes by KSHV. Science 274, 1739–1744.

Nakano, K., Isegawa, Y., Zou, P., Tadagaki, K., Inagi, R., Yamanishi, K., 2003. Kaposi's sarcoma-associated herpesvirus (KSHV)-encoded vMIP-I and vMIP-II induce signal transduction and chemotaxis in monocytic cells. Arch. Virol. 148, 871–890.

Niwa, H., Yamamura, K., Miyazaki, J., 1991. Efficient selection for high-expression transfectants with a novel eukaryotic vector. Gene 108, 193–199.

Schalling, M., Ekman, M., Kaaya, E.E., Linde, A., Biberfeld, P., 1995. A role for a new herpes virus (KSHV) in different forms of Kaposi's sarcoma. Nat. Med. 1, 707–708.

Soulier, J., Grollet, L., Oksenhendler, E., Cacoub, P., Cazals-Hatem, D., Babinet, P., d'Agay, M.F., Clauvel, J.P., Raphael, M., Degos, L., et al., 1995. Kaposi's sarcoma-associated herpesvirus-like DNA sequences in multicentric Castleman's disease. Blood 86, 1276–1280.

Sun, R., Lin, S.F., Staskus, K., Gradoville, L., Grogan, E., Haase, A., Miller, G., 1999. Kinetics of Kaposi's sarcoma-associated herpesvirus gene expression. J. Virol. 73, 2232–2242.

Wang, J.M., McVicar, D.W., Oppenheim, J.J., Kelvin, D.J., 1993. Identification of RANTES receptor on human monocytic cells: competition of binding and desensitization by homologous chemotactic cytokines. J. Exp. Med. 177, 699–705.

J Infect Chemother
DOI 10.1007/s10156-010-0101-5

ORIGINAL ARTICLE

Comparison of the influence of four classes of HIV antiretrovirals on adipogenic differentiation: the minimal effect of raltegravir and atazanavir

Rumi Minami · Masahiro Yamamoto · Soichiro Takahama · Hitoshi Ando · Tomoya Miyamura · Eiichi Suematsu

Received: 12 March 2010 / Accepted: 12 July 2010

Abstract Antiretroviral therapy for HIV infection is associated with lipodystrophy. However, raltegravir (RAL), a new integrase inhibitor, and atazanavir (ATV), a new generation of protease inhibitor (PI), have not been reported to significantly induce metabolic abnormalities in some clinical studies. The aim of this study was to investigate the influence and molecular mechanisms of RAL and compared it with the other three classes of ARVs (nucleoside reverse-transcriptase inhibitors; NRTI, nonnucleoside reverse-transcriptase inhibitor; NNRTI, and PI) on adipogenesis using 3T3-L1 cells. RAL and ATV had minimal effects on the lipid metabolism of 3T3-L1 cells. NRTI induced a moderate change, and NNRTI and some PIs induced a severe reduction in cell lipid content. These ARVs induced a decrease in the expression of genes associated with lipogenic transcription factors (sterol regulatory-element-binding protein-1c, CAAT box enhancer-binding protein-α, and peroxisome proliferator-activated receptor-γ). The differentiated 3T3-L1 cells were less sensitive to ARV-induced metabolic disturbance than were predifferentiated cells. RAL and ATV did not significantly affect the lipid metabolism in our in vitro study. The other ARVs had a direct influence on adipocytes. Degree and underlying mechanisms of metabolic disturbance differed among different ARVs. These data suggest that the distinct metabolic side-effect profiles of ARVs are a consequences of their differential effects on the adipocyte physiology. A better understanding of the mechanism of ARV-induced metabolic abnormalities could lead to safer use of ARVs or selection of alternative agents for further clinical development.

Keywords HIV-1 · Antiretrovirals · Adipocyte · Lipodystrophy

R. Minami (✉) · M. Yamamoto · S. Takahama · H. Ando · T. Miyamura · E. Suematsu
Internal Medicine, Clinical Research Institute, National Hospital Organization, Kyushu Medical Center, 1-8-1 Jigyohama, Chuo-ku, Fukuoka 810-8563, Japan
e-mail: rrhh@kyumed.jp

Introduction

Highly active antiretroviral therapy (HAART) has helped to control HIV infections and the development of AIDS. However, this antiretroviral therapy (ART) is often associated with severe lipodystrophy, such as peripheral lipoatrophy, central fat accumulation, and hyperlipidemia, but the use of new-generation protease inhibitors (PIs) atazanavir (ATV), and the integrase inhibitor raltegravir (RAL), has been reported to be associated with a decrease in hyperlipidemia [1] and reversal of lipodystrophy [2]. The cellular and molecular mechanisms underlying the metabolic abnormalities induced by ART are unclear, but many studies have shown that the pathogenesis of adipose cell dysfunction includes adverse effects on adipocyte differentiation status [3], survival [4], ability to secrete a variety of adipokines [5], mitochondrial function [6], and recovery from oxidative stress [7] induced by antiretrovirals (ARVs). Different ARVs might induce lipid abnormalities to a different degree though distinct mechanisms, and these properties could underlie the metabolic side-effect profile observed from the use of ARVs.

Adipocyte differentiation involves sequential and coordinated action of several transcription factors that regulate expression of adipocyte-specific genes [8]. Following the initial and transient increase in CAAT box enhancer-binding protein (C/EBP)-β and -δ, peroxisome-proliferator-activated receptor (PPAR)-γ, and C/EBP-α promote expression

Published online: 13 August 2010

of a number of adipose-specific markers, allowing acquisition of an enlarged, rounded shape and progressive accumulation of cytoplasmic triacylglycerol droplets. C/EBP-α is expressed early during adipogenesis and is involved in the induction of PPAR-γ. Coexpression of C/EBP-α and PPAR-γ has synergistic effects on adipogenic conversion, including lipid metabolism, adipokine secretion, and insulin sensitivity. Adipocyte differentiation is also enhanced by sterol regulatory-element-binding protein (SREBP)-1c. SREBP-1c activates PPAR-γ or related adipogenic transcription factors, thus leading to defective adipogenesis and insulin resistance. Therefore, PPAR-γ, C/EBP-α, and SREBP-1c act in concert to induce and maintain the adipocyte phenotype.

Many studies provide evidence that some PIs influence lipid metabolism by inhibiting degradation of adipogenic transcription factors, such as SREBPs [9, 10], C/EBP-α [11], and PPAR-γ [12, 13]. On the other hand, treatment with nucleoside reverse-transcriptase inhibitors (NRTIs) has been reported to affect mitochondrial functions [2, 14] by depleting mitochondrial DNA (mtDNA) and inhibiting transcription. Integrase inhibitor and the newer generation of PIs have been reported to exhibit antiviral efficacy without adverse affects on lipid metabolism [2, 15]. A re-examination of the molecular pharmacology and toxicology of ART, including these new drugs, may help explain the differences in the metabolic profiles observed among ART in clinical use and lead to the discovery of new drugs that will reduce the incidence of lipodystrophy and related metabolic complications in HIV-infected patients receiving HAART. This study first examined the influence of RAL and then compared it with the four classes of ARVs (NRTI, NNRTI, PI, and integrase inhibitor) with regard to lipid metabolism using well-characterized 3T3-L1 adipocytes [16].

Materials and methods

Cells

This study used the 3T3-L1 cell line, which is one of the most widely used and well-characterized models for studying adipocyte differentiation and function. After stimulation, 3T3-L1 preadipocytes show changes in gene expression and acquire adipocyte characteristics, such as a spherical shape and accumulation of triglyceride-rich lipid droplets, as signs of differentiation. The 3T3-L1 cells were purchased from the Japanese Collection of Research Bioresources (Tokyo, Japan) and maintained in Dulbecco's modified Eagle medium (DMEM) supplemented with 10% fetal bovine serum (FBS). Postconfluent cells were induced to differentiate by incubation with 0.5 mM 3-isobutylmethylxanthine and 1 μM dexamethasone for 2 days. This was followed by incubation with 10 μg/ml insulin for 2 days. The cells were then maintained in DMEM with 10% FBS for another 2 days. Antiretroviral drugs were added to the medium before and after the differentiation of 3T3-L1 cells.

Antiretroviral drugs

Zidovudine (AZT) was purchased from Calbiochem-Novabiochem. (California, USA). Abacavir (ABC), stavudine (d4T), didanosine (ddI), lamivudine (3TC), efavirenz (EFV), ritonavir (RTV), and nelfinavir (NFV) were purchased from Toronto Research Chemicals Inc. (Ontario, Canada). Atazanavir (ATV) was provided by Bristol-Myers Squibb Company (New York, USA). Lopinavir (LPV) was provided, by Abbott Laboratories (Illinois, USA). Amprenavir (APV) was provided by Glaxo SmithKline (North Carolina, USA). Raltegravir (RAL) was provided by Merck (New Jersey, USA). Drug stocks in dimethyl sulfoxide (DMSO) were stored at −20°C and diluted into culture media. Vehicle controls received the same final DMSO concentration as all drug-treated incubations (0.1%). The peak serum concentration (C_{max}) of each drug are as follows: AZT 1.07–3.03 μM, ABC 3.4–8.19 μM, d4T 2.14 μM, ddI 6.95 μM, 3TC 7.89–15.6 μM, EFV 14.2–28.8 μM, RTV 0.84–21.9 μM, NFV 5.0–8.6 μM, ATV 4.96–8.38 μM, LPV 8.22–22.2 μM, APV 6.68–16.2 μM, and RAL 10.44–11.15 μM. Cells were treated with 10 μM of ABC, AZT, d4T, ddI, 3TC, and NFV; and with 20 μM of EFV, RTV, ATV, LPV, APV, and RAL.

Quantitative real-time RT-PCR

Total cellular RNA was isolated from 3T3-L1 cells using QIAamp RNA Blood Mini (QIAGEN, Tokyo, Japan), including treatment with DNase. Complementary DNA (cDNA) was generated from the RNA using TAKARA RNA Polymerase Chain Reaction (PCR) kit (TAKARA BIO, Shiga, Japan). Real-time PCR was conducted with LineGene33 (BioFlux, Tokyo, Japan) using SYBR Green Realtime PCR Master Mix (TOYOBO Co, Osaka, Japan). The copy numbers of β-actin were determined in every sample tested as internal control to normalize DNA input. The ratio of the normalized mean value for drug-treated samples was calculated and is indicated in the graphs.

Oil red O staining

The cellular lipid content was assessed by lipid staining with Oil red O. Staining was quantified at 490 nm after solubilization using an Adipogenesis Assay Kit (Chemicon International, California, USA).

Quantitation of 8-OHdG in culture medium

The levels of 8-hydroxy-2′-deoxyguanosine (8-OHdG) in the culture medium were determined using a competitive enzyme-linked immunosorbent assay (ELISA) kit (DNA Damage ELISA Kit; Assay Designs Stressgen, Michigan, USA).

Statistical analysis

Results were reproduced in at least three independent experiments and are presented as mean ± standard error (SE). The Fisher least significant difference (LSD) post hoc test was used for multiple comparisons if analysis of variance (ANOVA) was significant. In all statistical comparisons, a P value of <0.05 was considered to be significant.

Results

Effect of ARVs on lipid content in 3T3-L1 cells

Effects of ARVs on dyslipidemia and lipodystrophy differ among ART regimens, but it is nearly impossible to fully assess the separate effects of each class of drug from the clinical data because patients almost always receive a combination of several classes of ARVs. As a result, in vitro models were used to examine the exact influence of the individual drugs on adipocyte development or metabolism using well-characterized preadipocyte 3T3-LI cells. Lipid accumulation in predifferentiated 3T3-L1 cells was dramatically decreased by NFV and mildly decreased by ABC, AZT, d4T, EFV, LPV, and APV (Fig. 1).

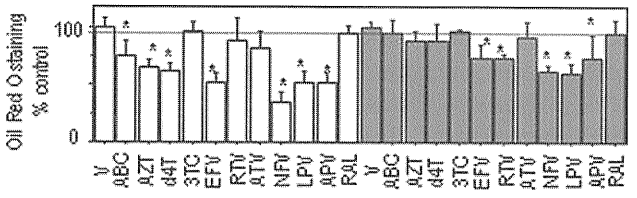

Fig. 1 Effect of antiretrovirals (ARVs) on triglyceride accumulation during 3T3-L1 adipose conversion. From confluence (day 0), 3T3-L1 cells were treated with differentiation medium in the absence (control) or presence of vehicle or various ARVs. To compare the effects of ARVs on preadipocytes with mature adipocytes, ARVs were added to the medium on day 0, when 3T3-L1 cells were still preadipocytes (*white bar*), or on day 6, when 3T3-L1 cells differentiate into mature adipocytes (*gray bar*). On day 7, the cells were stained with Oil red O. Staining was quantified at 490 nm after solubilization and expressed as percent ± standard error (SE) of the control. P values were evaluated by the Fisher least significant difference (LSD) post hoc test. *V* vehicle, *ABC* abacavir, *AZT* zidovudine, *d4T* stavudine, *3TC* lamivudine, *EFV* efavirenz, *RTV* ritonavir, *ATV* atazanavir, *NFV* nelfinavir, *LPV* lopinavir, *APV* amprenavir, *RAL* raltegravir. $*P < 0.01$

It is possible that the effect of ARVs on adipocyte metabolism is different between preadipocytes and differentiated mature adipocytes because the differentiation of adipocytes involves the sequential and coordinated action of several transcription factors that regulate the expression of adipocyte-specific genes and proteins. Therefore, differentiated 3T3-L1 cells were also treated with ARVs and assessed for effects on lipid accumulation. The differentiated 3T3-L1 cells were less sensitive to the effects of ARVs on lipid accumulation level than on immature 3T3-L1 cells. Lipid accumulation in mature 3T3-L1 cells was reduced by EFV, RTV, NFV, LPV, and APV (Fig. 1). On the other hand, RAL had little effect on lipid accumulation in both the immature and mature 3T3-L1 cells.

Effect of ARVs on lipogenic gene expression in 3T3-L1 cells

As shown in Fig. 1, several ARVs reduced lipid accumulation to different degrees. This suggests that various mechanisms are involved in the regulation of lipid accumulation and that different drugs might induce lipid abnormalities through distinct mechanisms. The key lipogenic transcription factors, including SREBP-1c (Fig. 2a), C/EBP-α (Fig. 2b), C/EBP-β (Fig. 2c), and PPAR-γ (Fig. 2d) were investigated to determine the primary cellular mechanisms that underlie these ARV-mediated lipid abnormalities. Treatment with several of the ARVs resulted in marked decreases in the expression of messenger RNAs (mRNAs) for C/EBP-α and SREBP-1c in predifferentiated 3T3-L1 cells (ABC, AZT, d4T, EFV, NFV, LPV, and APV for C/EBP-α; ABC, AZT, d4T, 3TC, EFV, NFV, LPV, and APV for SREBP-1c), and differentiated 3T3-L1 cells (AZT, d4T, EFV, RTV, NFV, LPV, and APV for C/EBP-α; ABC, d4T, 3TC, EFV, NFV, LPV, and APV for SREBP-1c) (Fig. 2). Expression of C/EBP-α and SREBP-1c was not affected by RTV, ATV, or RAL in predifferentiated 3T3-L1 cells. Predifferentiated 3T3-L1 cells were more sensitive to these ARVs than differentiated 3T3-L1 cells, but only RTV had a little stronger effect in the differentiated 3T3-L1 cells than in the predifferentiated cells on C/EBP-α expression. Effects of ARVs on C/EBP-α were similar to those on SREBP-1c. PPAR-γ was also down-regulated by EFV and some PIs (NFV, LPV, APV) but not by NRTIs (ABC, AZT, d4T, 3TC). ATV- and RAL-treated cells remained relatively quiescent. C/EBP-β, which is expressed early during adipogenesis, was not affected by any of the ARVs.

Effect of ARVs on oxidative stress in 3T3-L1 cells

Increased oxidative stress is associated with obesity-related disorders [17], and some ARVs increase oxidative stress in adipocytes in vitro [18] and in vivo [19]. Our study

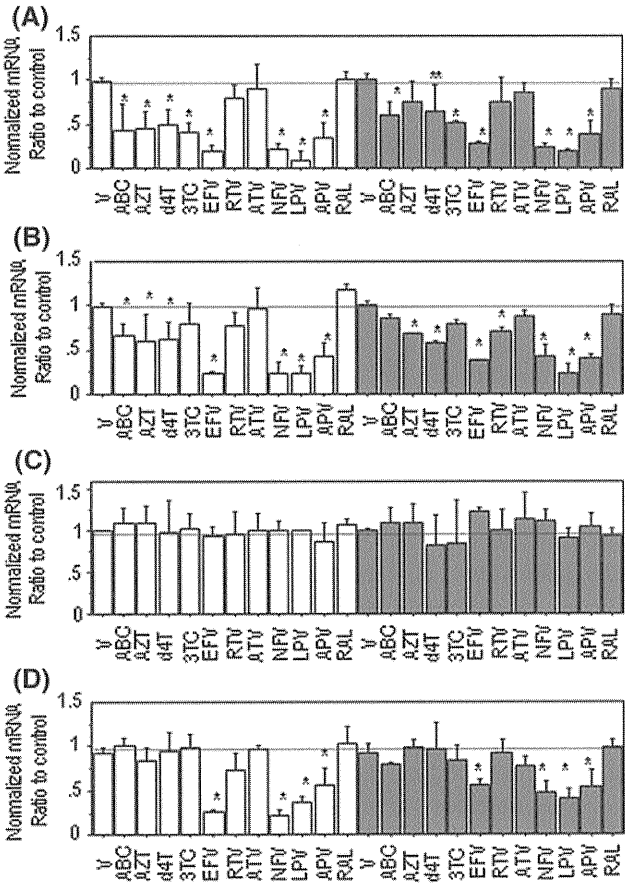

Fig. 2 Effect of antiretrovirals (ARVs) on lipogenic gene expression in 3T3-L1 cells. From confluence (day 0), 3T3-L1 cells were treated with differentiation medium in the absence (control) or presence of vehicle or various ARVs. To compare the effects of ARVs on preadipocytes with mature adipocytes, ARVs were added to the medium on day 0, when 3T3-L1 cells are still preadipocytes (*white bar*), or on day 6, when 3T3-L1 cells differentiate into mature adipocytes (*gray bar*). On day 7, total RNA was prepared, and messenger RNA (mRNA) levels were determined by real-time reverse-transcriptase polymerase chain reaction (RT-PCR). The results shown are after correction for the levels of β-actin mRNA and were normalized to the controls. *P* values were evaluated by Fisher's least significant difference (LSD) post hoc test. **a** sterol regulatory-element-binding protein, **b** CAAT box enhancer-binding protein-α, **c** C/EBP-β, **d** peroxisome-proliferator-activated receptor-γ. *V* vehicle, *ABC* abacavir, *AZT* zidovudine, *d4T* stavudine, *3TC* lamivudine, *EFV* efavirenz, *RTV* ritonavir, *ATV* atazanavir, *NFV* nelfinavir, *LPV* lopinavir, *APV* amprenavir, *RAL* raltegravir. $^{*}P < 0.01$, $^{**}P < 0.05$

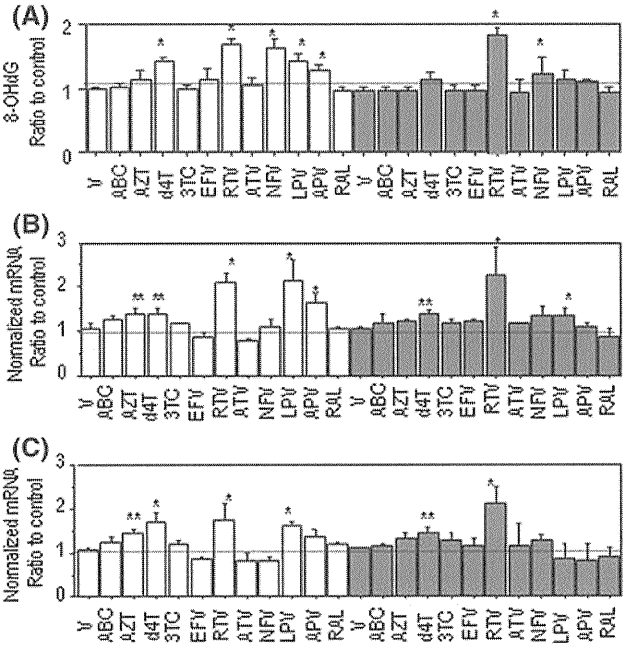

Fig. 3 Effect of antiretrovirals (ARVs) on oxidative stress in 3T3-L1 cells. From confluence (day 0), 3T3-L1 cells were treated with differentiation medium in the absence (control) or presence of vehicle or various ARVs. To compare the effects of ARVs on preadipocytes with mature adipocytes, ARVs were added to the medium on day 0, when 3T3-L1 cells are still preadipocytes (*white bar*), or on day 6, when 3T3-L1 cells differentiate to mature adipocytes (*gray bar*). **a** For the assay of 8-OHdG, each supernatant was collected at day 7. Then, concentrations of 8-OHdG were determined using an enzyme-linked immunosorbent assay (ELISA). Results shown were normalized to the controls and represent the mean ± standard error (SE). On day 7, total RNA was prepared, and messenger RNA (mRNA) levels were determined by real-time reverse-transcriptase polymerase chain reaction (RT-PCR). Effects of the drugs on **b** superoxide dismutase (SOD) and **c** catalase (CAT) were also examined. The results shown were obtained after correction for the levels of β-actin mRNA and were also normalized to the controls. Data are presented as the mean ± standard error (SE). *P* values were evaluated by the post hoc test. *V* vehicle, *ABC* abacavir, *AZT* zidovudine, *d4T* stavudine, *3TC* lamivudine, *EFV* efavirenz, *RTV* ritonavir, *ATV* atazanavir, *NFV* nelfinavir, *LPV* lopinavir, *APV* amprenavir, *RAL* raltegravir. $^{*}P < 0.01$

investigated the influence of the four classes of ARVs on the production of oxidative stress by measuring 8-OHdG in the culture medium. This compound is a modified nucleoside base, which is associated with reactive oxygen species (ROS) and used as a biomarker of oxidative stress. The level of 8-OHdG was increased in the culture medium of predifferentiated 3T3-L1 cells by d4T, RTV, NFV, LPV, and APV and was increased in differentiated 3T3-L1 cells by RTV and NFV (Fig. 3a). Expression of antioxidant enzymes, including superoxide dismutase (SOD, Fig. 3b) and catalase (CAT, Fig. 3c) was also investigated. Generally, oxidative stress, such as that induced by the free-radical superoxide, stimulates the expression of SOD and CAT. Expression of SOD mRNA was increased by the addition of AZT, d4T, RTV, LPV, and APV in predifferentiated 3T3-L1 cells; and d4T, RTV, and LPV in differentiated 3T3-L1 cells. Expression of CAT mRNA was increased by the addition of AZT, d4T, RTV, and LPV in predifferentiated 3T3-L1 cells and of d4T and RTV in differentiated 3T3-L1 cells. Neither SOD mRNA nor CAT mRNA was increased by the addition of ABC, 3TC, EFV, ATV, NFV, or RAL in predifferentiated and differentiated cells. These results and previous studies indicate that the

influence of ARVs on oxidative stress or the antioxidant system differs based upon the class and particular structure of the ARV.

Discussion

ART has been involved in the emergence of a metabolic disorder with potentially severe consequences, but the use of new-generation PIs ATV and the integrase inhibitor RAL has been reported to be associated with a decrease in hyperlipidemia [1] and a reversal of lipodystrophy [2]. Most previous studies examined one or a few classes of ARVs, and each study used different cell systems. Therefore, it is difficult to compare the effects of each drug. Our study investigated the effect of four classes of ARVs (NRTIs, NNRTI, PIs, and integrase inhibitor) using pre- and post-differentiated 3T3-L1 cells. We were especially interested in determining the effects of RAL and ATV compared with other ARVs in order to obtain a better understanding of the molecular basis for the more favorable metabolic side-effect profile associated with RAL and ATV. This is the first study to investigate the effects of RAL on the cellular and molecular regulation of adipocytes.

Expression of C/EBP-α, PPAR-γ, and SREBP-1c were strongly inhibited by some PIs, mildly inhibited by NNRTI and NRTIs, and minimally affected by ATV, RAL, and RTV. These results and the fact that RTV decreased lipid accumulation and increased oxidative stress in mature 3T3-L1 cells more than in predifferentiated cells suggest that the effect of RTV occurs relatively late in adipocyte differentiation. C/EBP-β, which is expressed during early adipogenesis, was not affected by ARVs, suggesting that molecular targets affected by the antiadipogenic properties of ARVs are probably located downstream of this adipogenic transcription factor. This is consistent with previous reports that some ARVs block adipocyte differentiation by inhibiting the expression of C/EBP-α and PPAR-γ [3, 12, 13] or by impairing SREBP-1 intranuclear localization [9, 20]. These findings indicate that altered functions of PPARγ, C/EBP-α, and SREBP-1c play a role in ARV-related dystrophy.

Increased oxidative stress is also considered to contribute to metabolic abnormalities caused by ARVs. Several reports indicate that ROS production in response to ARVs probably results from increased mitochondrial oxidative stress [7, 14]. The marker of oxidative stress, 8-OHdG, was increased by d4T, RTV, NFV, LPV, and APV, and the antioxidant pathway was impaired by NFV. These results indicate that increased oxidative stress by ARVs is due to activation of ROS production and an impaired antioxidant system. Oxidative stress also contributed to ARV-induced lipogenic abnormalities.

Mature 3T3-L1 cells were less sensitive to the lipid-reducing effect of ARVs than were predifferentiated 3T3-L1 cells, and similar results were obtained with regard to the inhibitory effect of ARVs on the expression of lipogenic transcription factors and some oxidative stress markers. One explanation for the differences between preadipocytes and mature adipocytes is that the more differentiated adipocytes have pathways that could enable cells to escape from ARV-induced blockade of the lipogenic pathway, or they may have a system that inactivates and/or decreases the intracellular level of ARVs.

It is notable that the intracellular events reflect lipoatrophy in the form of depleted adipocyte triglyceride stores, and the extent that each ARV influences the adipocytes was in proportion to that observed in clinical manifestations, although functional links between the molecular mechanism and the observed metabolic alterations are still not fully understood. It is certain that metabolic disorder is affected by numerous other modifiers, including genetic predisposition, diet and lifestyle, and HIV-1 infection. However, some features can be avoided by careful selection of ARVs and thus can be effectively treated.

In conclusion, different ARVs acted through distinct mechanisms to induce disruption of adipocyte differentiation and function to different degrees through distinct mechanisms. Whereas most of ARVs affected lipid accumulation, RAL and ATV had no influence on lipid metabolism in our in vitro study. A greater understanding of the mechanisms underlying the development of this metabolic effect could lead to safer ARVs while indicating the best treatment for these metabolic side effects of ARVs.

Acknowledgments We are grateful to Ms. Mariko Takahashi for her valuable technical support. This study was partly supported by Health Science Research Grants on HIV/AIDS from the Ministry of Health, Labor and Welfare of the Japanese Government. The sponsor had no role in study design, data collection, data analysis, data interpretation, or writing of the report.

References

1. Stanley TL, Joy T, Hadigan CM, Liebau JG, Makimura H, Chen CY, et al. Effects of switching from lopinavir/ritonavir to atazanavir/ritonavir on muscle glucose uptake and visceral fat in HIV-infected patients. AIDS. 2009;23:1349–57.
2. Haerter G, Manfras BJ, Mueller M, Kern P, Trein A. Regression of lipodystrophy in HIV-infected patients under therapy with the new protease inhibitor atazanavir. AIDS. 2004;18:952–5.
3. Stankov MV, Schmidt RE, Behrens GM. German Competence Network HIV/AIDS. Zidovudine impairs adipogenic differentiation through inhibition of clonal expansion. Antimicrob Agents Chemother. 2008;52:2882–9.
4. Kim RJ, Wilson CG, Wabitsch M, Lazar MA, Steppan CM. HIV protease inhibitor-specific alterations in human adipocyte differentiation and metabolism. Obesity (Silver Spring). 2006; 14:994–1002.

5. Cianflone K, Zakarian R, Stanculescu C, Germinario R. Protease inhibitor effects on triglyceride synthesis and adipokine secretion in human omental and subcutaneous adipose tissue. Antivir Ther. 2006;11:681–91.
6. Flint OP, Noor MA, Hruz PW, Hylemon PB, Yarasheski K, Kotler DP, et al. The role of protease inhibitors in the pathogenesis of HIV-associated lipodystrophy: cellular mechanisms and clinical implications. Toxicol Pathol. 2009;37:65–77.
7. Lagathu C, Eustace B, Prot M, Frantz D, Gu Y, Bastard JP, et al. Some HIV antiretrovirals increase oxidative stress and alter chemokine, cytokine or adiponectin production in human adipocytes and macrophages. Antivir Ther. 2007;12:489–500.
8. Rosen ED, Walkey CJ, Puigserver P, Spiegelman BM. Transcriptional regulation of adipogenesis. Genes Dev. 2000; 14:1293–307.
9. Bastard JP, Caron M, Vidal H, Jan V, Auclair M, Vigouroux C, et al. Association between altered expression of adipogenic factor SREBP1 in lipoatrophic adipose tissue from HIV-1-infected patients and abnormal adipocyte differentiation and insulin resistance. Lancet. 2002;359:1026–31.
10. Hirano Y, Yoshida M, Shimizu M, Sato R. Direct demonstration of rapid degradation of nuclear sterol regulatory element-binding proteins by the ubiquitin-proteasome pathway. J Biol Chem. 2001;276:36431–7.
11. Dowell P, Flexner C, Kwiterovich PO, Lane MD. Suppression of preadipocyte differentiation and promotion of adipocyte death by HIV protease inhibitors. J Biol Chem. 2000;275:41325–32.
12. Parker RA, Flint OP, Mulvey R, Elosua C, Wang F, Fenderson W, et al. Endoplasmic reticulum stress links dyslipidemia to inhibition of proteasome activity and glucose transport by HIV protease inhibitors. Mol Pharmacol. 2005;67:1909–19.
13. Caron M, Vigouroux C, Bastard JP, Capeau J. Antiretroviral-related adipocyte dysfunction and lipodystrophy in HIV-infected patients: alteration of the PPARgamma-dependent pathways. PPAR Res. 2009;2009:507141.
14. Stankov MV, Lücke T, Das AM, Schmidt RE, Behrens GM. Relationship of mitochondrial DNA depletion and respiratory chain activity in preadipocytes treated with nucleoside reverse transcriptase inhibitors; German Competence Network HIV/AIDS. Antivir Ther. 2007;12:205–16.
15. Eron JJ, Young B, Cooper DA, Youle M, Dejesus E, Andrade-Villanueva J, et al. Switch to a raltegravir-based regimen versus continuation of a lopinavir–ritonavir-based regimen in stable HIV-infected patients with suppressed viraemia (SWITCHMRK 1 and 2): two multicentre, double-blind, randomised controlled trials. Lancet. 2010;375:396–407.
16. Green H, Kehinde O. An established preadipose cell line and its differentiation in culture. Cell. 1975;5:19–27.
17. Kamigaki M, Sakaue S, Tsujino I, Ohira H, Ikeda D, Itoh N, et al. Oxidative stress provokes atherogenic changes in adipokine gene expression in 3T3-L1 adipocytes. Biochem Biophys Res Commun. 2006;339:624–32.
18. Ben-Romano R, Rudich A, Etzion S, Potashnik R, Kagan E, Greenbaum U, et al. Nelfinavir induces adipocyte insulin resistance through the induction of oxidative stress: differential protective effect of antioxidant agents. Antivir Ther. 2006;11:1051–60.
19. Masiá M, Padilla S, Bernal E, Almenar MV, Molina J, Hernández I, et al. Influence of antiretroviral therapy on oxidative stress and cardiovascular risk: a prospective cross-sectional study in HIV-infected patients. Clin Ther. 2007;29:1448–55.
20. El Hadri K, Glorian M, Monsempes C, Dieudonné MN, Pecquery R, Giudicelli Y, et al. In vitro suppression of the lipogenic pathway by the nonnucleoside reverse transcriptase inhibitor efavirenz in 3T3 and human preadipocytes or adipocytes. J Biol Chem. 2004;279:15130–41.

Watanabe et al. BMC Infectious Diseases 2011, 11:146
http://www.biomedcentral.com/1471-2334/11/146

BMC Infectious Diseases

RESEARCH ARTICLE Open Access

Cellular HIV-1 DNA levels in patients receiving antiretroviral therapy strongly correlate with therapy initiation timing but not with therapy duration

Dai Watanabe[1*], Shiro Ibe[2], Tomoko Uehira[1], Rumi Minami[3], Atsushi Sasakawa[1], Keishiro Yajima[1], Hitoshi Yonemoto[1], Hiroki Bando[1], Yoshihiko Ogawa[1], Tomohiro Taniguchi[1], Daisuke Kasai[1], Yasuharu Nishida[1], Masahiro Yamamoto[3], Tsuguhiro Kaneda[4] and Takuma Shirasaka[1]

Abstract

Background: Viral reservoir size refers to cellular human immunodeficiency virus-1 (HIV-1) DNA levels in $CD4^+$ T lymphocytes of peripheral blood obtained from patients with plasma HIV-1-RNA levels (viral load, VL) maintained below the detection limit by antiretroviral therapy (ART). We measured HIV-1 DNA levels in $CD4^+$ lymphocytes in such patients to investigate their clinical significance.

Methods: $CD4^+$ T lymphocytes were isolated from the peripheral blood of 61 patients with a VL maintained at less than 50 copies/ml for at least 4 months by ART and total DNA was purified. HIV-1 DNA was quantified by nested PCR to calculate the copy number per 1 million $CD4^+$ lymphocytes (relative amount) and the copy number in 1 ml of blood (absolute amount). For statistical analysis, the Spearman rank or Wilcoxon signed-rank test was used, with a significance level of 5%.

Results: CD4 cell counts at the time of sampling negatively correlated with the relative amount of HIV-1 DNA (median = 33 copies/million $CD4^+$ lymphocytes; interquartile range [IQR] = 7-123 copies/million $CD4^+$ lymphocytes), but were not correlated with the absolute amounts (median = 17 copies/ml; IQR = 5-67 copies/ml). Both absolute and relative amounts of HIV-1 DNA were significantly lower in six patients in whom ART was initiated before positive seroconversion than in 55 patients in whom ART was initiated in the chronic phase, as shown by Western blotting. CD4 cell counts before ART introduction were also negatively correlated with both the relative and absolute amounts of HIV-1 DNA. Only the relative amounts of HIV-1 DNA negatively correlated with the duration of VL maintenance below the detection limit, while the absolute amounts were not significantly correlated with this period.

Conclusions: The amounts of cellular HIV-1 DNA in patients with VLs maintained below the detection limit by the introduction of ART correlated with the timing of ART initiation but not with the duration of ART. In addition, $CD4^+$ T lymphocytes, which were newly generated by ART, diluted latently infected cells, indicating that measurements of the relative amounts of cellular HIV-1 DNA might be underestimated.

* Correspondence: dai@onh.go.jp
[1]AIDS Medical Center, National Hospital Organization Osaka National Hospital, Osaka, Japan
Full list of author information is available at the end of the article

Background

Anti-human immunodeficiency virus (HIV) drugs can suppress viral replication but cannot directly eliminate latently HIV-1-infected cells. Replication-competent HIV-1 can persist in a stable latent reservoir in $CD4^+$ T lymphocytes and monocytes, thus carrying integrated HIV-1 DNA. Among these cells, resting memory $CD4^+$ T lymphocytes constitute a major latent reservoir [1]. Siliciano et al. calculated the number of latently infected cells as the frequency of replication-competent virus per 1 million $CD4^+$ lymphocytes in peripheral blood and reported that their half-life was about 44 months [2]. The number of latently infected cells in an HIV-1-infected patient's body is estimated to be approximately 1 million [3]. The report concluded that an HIV-infected patient's body undergoing anti-HIV therapy (ART) would take 73.4 years for complete viral elimination; thus, ART would need to be continued for the rest of the patient's life [4]. However, the method for calculating the frequency of replication-competent virus in this previous report is not necessarily sensitive enough. An alternative method for estimating the viral reservoir size of a patient receiving ART is to quantify cellular HIV-1 DNA in infected cells.

Many studies have reported the amount of cellular HIV-1 DNA in peripheral blood. In particular, the recent use of real-time PCR has allowed the straightforward and accurate measurement of HIV-1 DNA. It also enables us to distinguish all forms of intracellular HIV-1 DNA, including integrated and unintegrated linear DNA, as well as 1-long terminal repeat (LTR) and 2-LTR circles. The total HIV-1 DNA in peripheral blood mononuclear cells (PBMC) and in $CD4^+$ lymphocytes after prolonged viral suppression largely corresponds to integrated HIV-1 DNA [5,6]. This evidence indicates that integrated HIV-1 DNA is the most stable form in patients receiving ART, and that viral reservoir sizes can therefore be estimated by examining the amounts of cellular HIV-1 DNA.

We reported the detection limit of real-time PCR, using the LightCycler system, to be 500 copies per 1 million cells in peripheral blood; therefore, HIV-1 DNA in 30% of the patients receiving ART could not be quantified using the conventional real-time PCR method [7]. In a subsequent study, we improved the detection level of HIV-1 DNA levels with real-time PCR by including a pre-amplification step in the first PCR, followed by quantification with a second PCR [8]. Specifically, we PCR-amplified the β2-microglobulin (β2 M) gene and HIV-1 DNA simultaneously in the same tube, quantified the products by TaqMan PCR, and then determined the amounts of HIV-1 DNA using the copy number of amplified HIV-1 DNA and the amplification efficiency of β2 M. This method improved the detection limit to 2 copies/10^6 cells. Here, we measured the amount of HIV-1 DNA in $CD4^+$ lymphocytes in the peripheral blood using this novel, highly sensitive method in HIV patients who have undergone ART for a prolonged period, and in whom the plasma HIV-1 RNA levels (viral load, VL) remained undetectable.

Methods

Patients and study design

Adult patients visiting either the Osaka National Hospital or the Kyushu Medical Center and whose VL levels remained below the detection limit (50 copies/ml) for 4 months or longer were included in this cross-sectional analysis of an open-labeled cohort of HIV-1-infected patients successfully treated with ART. Written informed consent for collection of peripheral blood was obtained from 69 patients. Of these patients, 8 patients with a history of rebound of VLs (>400 copies/ml) were excluded from the study. This study was reviewed and approved by the institutional review boards of the Osaka National Hospital and relevant institutions.

Estimation of the number of CD4+ T lymphocytes (CD4 cell count) and HIV-1 VL

CD4 cell counts were measured by flow cytometry using the whole-blood lysis method. VLs were measured using the reverse transcription PCR method (AMPLICOR HIV-1 monitor test, Roche Molecular Diagnostic), with a detection limit of 50 copies/ml, according to the manufacturer's instructions. Serum anti-HIV-1 antibody levels were detected using LAV Blot I (Bio-Rad Laboratories). Sera were determined to be positive for the antibody according to the criteria of the World Health Organization.

Isolation of CD4-positive T lymphocytes and DNA extraction

Peripheral blood was collected with an EDTA blood collecting tube. CD4-positive T lymphocytes were isolated from whole blood using StemSep column chromatography (Stem Cell Technologies). The collected cells were then washed with phosphate-buffered saline and resuspended. The purity of CD4-positive T lymphocytes was more than 98% by flow cytometry. For DNA extraction, 1-5 × 10^6 cells were used. DNA was extracted using the QIAamp DNA Blood Mini Kit (QIAGEN) according to the manufacturer's instructions.

Quantification of HIV-1 DNA

HIV-1 DNA was quantified by real-time PCR as previously reported [8]. A second round of PCR was conducted using the extracted DNA as a template. First, the